SYNTHESIS OF DOXORUBICIN-PROTEIN CONJUGATES VIA COBALT COORDINATION CHEMISTRY: CONJUGATES OF TRANSFERRIN AND IMMUNOGLOBULIN G

A THESIS

SUBMITTED IN PARTIAL FULFILLMENT OF THE REQUIREMENTS

FOR THE DEGREE OF MASTER OF SCIENCE

IN THE GRADUATE SCHOOL OF THE

TEXAS WOMAN'S UNIVERSITY

DEPARTMENT OF CHEMISTRY AND BIOCHEMISTRY

COLLEGE OF ARTS AND SCIENCES

BY

JUAN JOSE CARVAJAL DE LUNA B.S.

DENTON, TEXAS

DECEMBER 2021

DEDICATION

I would like to dedicate my thesis to the memory of my grandmother, Maria del Carmen Gonzalez. I miss her every day, but I know she would have been proud of me.

To my grandfather, Leobardo de Luna. For always supporting my dreams and advising me.

To my belove mother, Edith de Luna. For always being there when I need her and all her unconditional support.

To my lovely wife, Claudia Garcia. For her constant encouragement, and motivation.

ACKNOWLEDGMENTS

I would like to thank my mentor Dr. Robby Petros, for his endless guidance. The knowledge shared with me, and your teaching made an impact in my career. Thank you for believing in me and giving me the opportunity to be part of your research group. I sincerely would like to thank the faculty in the chemistry and biochemistry department for keep me motivated, always sharing your expertise, and making my education at Texas Woman's University such a unique experience. Thank you, Dr. John Beaty, for your expertise with the HPLC, and the career advising. I would like to thank Dr. Nasrin Kohan, for your constant support and for truly caring. Special thanks to Courtney Hawkins for always helping me with registration and for giving me the opportunity to T.A. I would like to thank Dr. Manal Omary for reminding to think outside the box and her constant encouragement. I would like to thank Lindsey Hynes for her constant assistance with DSC and providing laboratory materials. I would like to thank Karen Underbrink from Dr. Bergel's group for her time teaching me how to do cell cultures.

Thank you to my committee, Dr. Robby Petros, Dr. Nasrin Kohan, and Dr. Richard Sheardy, for the constant assistance and for all your teachings.

I would like to thank my grandparents for never stop believing in me and always being supportive. I would like to thank my wife for all the motivation and inspiration she provides me. Finally, I would like to thank my mother for never giving up on me and regardless of the situation, she has always been there for me.

ABSTRACT

JUAN JOSE CARVAJAL DE LUNA

SYNTHESIS OF DOXORUBICIN-PROTEIN CONJUGATES VIA COBALT COORDINATION CHEMISTRY: CONJUGATES OF TRANSFERRIN AND IMMUNOGLOBULIN G

DECEMBER 2021

Protein-drug conjugates are a rapidly expanding family of therapeutics that hold significant potential to ameliorate off-target toxic effects commonly observed in patients undergoing chemotherapy. chemotherapy. In this context, the protein acts as a nanoscale delivery vector that alters the biodistribution of the drug upon administration by restricting its unhindered distribution in vivo. This thesis explores the use of cobalt coordination chemistry in the synthesis of doxorubicin-protein conjugates. Previous work has shown that cobalt can be used to crosslink amine-containing molecules in a reversible reaction that only utilizes the lone pair of electrons on nitrogen to form a dative bond with cobalt. Doxorubicin was chosen for initial studies because it contains a primary amine that could be crosslinked with lysine residues on a protein to form a protein-drug conjugate. Conjugates of dox with albumin, transferrin, and immunoglobulin G were investigated to demonstrate the broad applicability of the method for bioconjugation reactions. Drug loading was investigated by high performance liquid chromatography and the conjugates further characterized by dynamic light scattering, calorimetry, and

cytotoxicity. Details of the effects of reaction conditions on synthesis of stable conjugates are discussed.

TABLE OF CONTENTS

Page

DEDICATION ii

ACKNOWLEDGMENTS iii

ABSTRACT iv

TABLE OF CONTENTS vi

LIST OF TABLES viii

LIST OF FIGURES ix

Chapter

I. INTRODUCTION 1

Introduction 1
Nanoparticles - Polymer Drug Conjugates 2
Doxorubicin (Adriamycin) 5
Transferrin and Immunoglobulin G 7
Cobalt as the Linker 8
Analytical Theories 9
Dialysis Cassette 9
High Performance Liquid Chromatography 9
Quasi-Elastic Light Scattering 10
Cytotoxicity 11
Differential Scanning Calorimetry 11

II. METHODOLOGY AND MATERIALS 13

Synthesis of Protein Drug Conjugates 13
HSA-Dox Conjugate Parameters 14
Different Cobalt Oxidation Time 14
Change in pH 15

Change in Cobalt Concentration 15
Change in Dox Concentration 16
Tf-Dox Conjugate and IgG-Dox Conjugate 17
Synthesis of Tf-Dox Conjugate 17
Synthesis of IgG-Dox Conjugate 18
Characterization of the Conjugates 18
Calibration Solution 18
Dialysis Cassette 19
HPLC 20
HPLC Method 21
QELS or DLS 21
DSC 22
Cytotoxicity 22

III. RESULTS 24

Synthesis and Characterization of Protein-Dox Conjugates 24
HPLC Studies 24
Different Cobalt Oxidation Times 24
UV-Vis and Fluorescence Wavelengths 28
Change in pH 33
Change in Cobalt Concentration 42
Change in Doxorubicin Concentration 47
Tf-Dox Conjugate and IgG-Dox Conjugate 50
Dynamic Light Scattering Studies 52
Differential Scanning Calorimetry Study 55
Cytotoxicity 56

IV. FINAL DISCOVERY 58

V. CLOSING STATEMENTS 60

REFERENCES 61

LIST OF TABLES

Table Page

1. HPLC Results from the Change In Oxidation Time 25

2. HPLC Results from the Calibration Curve 26

3. HPLC Results from Different pH Samples 39

4. HPLC Results from Change in Cobalt Concentration 43

5. HPLC Result from Calibration Curve Samples for Change in Cobalt Concentration, Change in Dox Concentration, Synthesis of IgG, and Synthesis of Tf 45

6. HPLC Results from Change in Dox Concentration 48

7. HPLC Results from Synthesis of IgG-Dox Conjugate and Tf-Dox Conjugate 51

8. DLS Results[a] 53

LIST OF FIGURES

Figure Page

1. Illustration of the bonding between Dox and the protein via cobalt coordination chemistry. 4

2. Illustration of the protein-Dox conjugate via cobalt coordination chemistry. 5

3. Chemical structure of doxorubicin. 7

4. HPLC absorbance chromatograms of cobalt oxidation time at 10 minutes, 4 hours, and 24 hours. 25

5. Calibration curve based on the bulk sample. 27

6. HPLC absorbance chromatograms of dilutions of the bulk sample. 27

7. Absorbance spectra of Dox and Dox in 1X PBS with Acetonitrile 29

8. Absorbance spectrum of 1X PBS 29

9. HPLC absorbance chromatograms of Dox in 1X PBS at different wavelengths. 30

10. HPLC absorbance chromatograms of 1X PBS Samples at 233 nm 31

11. HPLC absorbance chromatograms of 1X PBS and Dox in 1X PBS 31

12. HPLC chromatograms of absorbance signal and fluorescence signal from Dox at the same scale. 32

13. HPLC chromatograms of fluorescence signals from 1X PBS and Dox in 1X PBS. .. 33

14. Different pH samples before and after. The left picture is the initial set up of the experiment. The right picture is after 72 hours. The bulk sample of the samples with

cobalt after 72 hours had a higher red tint than the samples without cobalt. This indicates a higher release of Dox, which means a lower conjugation number. 34
15. Different pH samples after 10 days. 35
16. HPLC chromatograms of absorbance signals from solutions with different pH. 36
17. HPLC chromatograms of fluorescence signals from solutions with different pH. 37
18. Conjugation number for change in pH. 37
19. Dox-only samples. The left picture is the sample at the beginning of the experiment and the right picture is the sample after 72 hours. 38
20. HPLC absorbance chromatograms for calibration curve of change in pH. 40
21. Absorbance calibration curve for change in pH. 40
22. HPLC fluorescence detection chromatograms for calibration curve of change in pH 41
23. Fluorescence calibration curve for change in pH. 41
24. HPLC absorbance chromatograms from samples with different cobalt concentrations. 44
25. HPLC fluorescence detection chromatograms for samples with different cobalt concentrations. 45
26. HPLC absorbance chromatograms of calibration curve for change in cobalt concentration, change in Dox concentration, synthesis of IgG, and synthesis of Tf.. 46
27. HPLC fluorescence detection chromatograms of calibration curve for change in cobalt concentration, change in Dox concentration, synthesis of IgG, and synthesis of Tf. 46

28. Absorbance (left) and fluorescence detection (right) calibration curves for change in cobalt concentration, change in Dox concentration, synthesis of IgG, and synthesis of Tf. 47
29. HPLC absorbance chromatograms from samples with different Dox concentrations. 49
30. HPLC fluorescence detection chromatograms for samples with different Dox concentrations. 49
31. HPLC fluorescence detection chromatograms of bulk samples from IgG-Dox conjugate and Tf-Dox conjugate. The elution time of dox was at 3.8 min for both samples, but the dox peak of the IgG sample had a higher intensity. 50
32. HPLC absorbance chromatograms of bulk samples from IgG-Dox conjugate and Tf-Dox conjugate. The elution time of dox was at 3.8 min for both samples, but the dox peak of the IgG sample had a higher intensity. 51
33. Particle size distribution of HSA-Dox conjugate with no cobalt. 52
34. Particle size distribution of HSA-Dox conjugates with different amounts of cobalt, 26 µL Co (A), 52.5 µL Co (B), 78.5 µL Co (C), and 105 µL Co (D). 53
35. Particle size distribution of different concentration of Dox (A. 50 µL Dox, B. 100 µL Dox, C. 200 µL Dox, D. 400 µL Dox), Tf-Dox conjugate (E), and IgG-Dox conjugate(F). 54
36. DSC thermogram of Tf protein. The green line is the raw data, and the black graph is the Two State Scaled model used to calculate the T_m (84.80 ºC) and ΔH (566.9 KJ/mol). 55

37. DSC thermogram of Tf-Dox conjugate. The green line is the raw data, and the black graph is the Two State Scaled model used to calculate the T_m (84.83 ºC) and ΔH (565.2 KJ/mol). 56

38. Cell viability studies of IgG-Dox conjugate, Tf-Dox conjugate, and HSA-Dox conjugate in MCF-7 cells with MTS assay. 57

39. Dox and Dox dimer structures. 59

CHAPTER I

INTRODUCTION

Introduction

One of the major obstacles in life is to stay alive. There are many different diseases affecting humans. Some of them are treatable, while others remain an issue for our survival. There are also circumstances where some diseases have been eradicated.[1] One major cause of mortality worldwide is cancer.[2] Cancer is also the second leading cause of death in the United States of America.[2] According to statistics from the Global Cancer Observatory, the number of new cancer cases are expected to increase from 19.3 million cases in 2020 to 30.2 million by 2040.[3]

The available treatments against cancer are surgery, radiation therapy, chemotherapy, hormone therapy, targeted therapy, and transplantation of bone marrow, stem cell, and cord blood.[4] The method of treatment depends on the type of cancer and the location. Surgery is the most common treatment and most effective as it removes the actual tumor.[4] There are times when surgery cannot be performed due to the location or size of the tumor. Radiation therapy can be use by itself or in combination with other therapies. Radiation therapy causes fatigue on patients during the treatment. Targeted therapy uses drugs to target specific characteristic found in cancer cells that are not found in healthy cells. Cancer cells can mutate to create immunity or develop a new growth path. Hormone therapy involves targeting of the hormones that some cancers utilize for

growth. Since not all cancers are dependent on hormones this therapy is only used for certain types of cancers. Chemotherapy uses chemicals to kill cancer cells. Chemotherapeutics target fast dividing cells, a common characteristic of cancer cells, but they fail to differentiate between healthy and cancer cells.[5] Chemotherapy can also be used in conjunction with other treatments or by itself. Chemotherapy can destroy cancer cells that have traveled to other parts of the body. The issue with chemotherapy is the side effects caused because the off-target toxicity. The drug used for chemotherapy depends on the type of cancer. There are different types of chemotherapeutic agents: alkylating agents, platinum drugs, antimetabolites, antitumor antibiotics, topoisomerase inhibitors, mitotic inhibitors, anticancer corticosteroids, asparaginase, and bortezomib. The dose of the drug is prescribed depending on the health of the patient, as these drugs might cause damage to the heart or other tissues. The drugs tend to have a short half-life while in circulation, due to their small size.[6] Consequently, they can escape circulation, causing side effects. In order to decrease or eliminate the off-target toxicity of the drugs, new approaches are being investigated. The use of nanoparticles for therapeutic use provides a more beneficial alternative.

Nanoparticles - Polymer Drug Conjugates

Nanoparticles can improve the delivery of drugs by increasing circulation half-life, reduce systemic toxicity, and provide selectivity to target cancer cells.[7] The size of the nanoparticles also plays an important challenge in their development for therapeutic use. The development of new blood vessels in tumors causes an increased permeability.

Tumors also tend to have a poor lymphatic drainage. The combination of the increase vascular permeability and the weak lymphatic drainage is called enhanced permeability and retention effect (EPR).[7–9] The EPR effect contributes to the passive accumulation of nanoparticles in tumors. The size is important because the blood vessels in the tumors contain pores with a size between 200 nm to 1200 nm.[8] Nanoparticles smaller than 30 nm are cleared by the renal excretion. Particles bigger than 200 nm risk being taken up by the mononuclear phagocytic system.[8] It has been observed that to take full advantage of the EPR effect nanoparticles need to have a size below 200 nm.[7–9] Active targeting of cancer cells can also be achieved by the use of antibodies, peptides, or other molecules. Cancer cells express receptors that are not found in the healthy cells, or they overexpress some receptors.

Nanoparticles for pharmaceutical use are defined as "solid colloidal particles ranging in size from 1 nm to 1,000 nm".[7] The first reported nanoparticle dates back to 1955, a polymer-drug conjugate. A polymer-drug conjugate is a drug covalently linked to a polymer, such as a protein. The first polymer-drug consisted of mescaline linked to polyvinylpyrrolidone by a short peptide linker. Two important remarks were observed: Without the use of the short peptide linker, there was no release of mescaline *in vivo*, and when the short peptide linker was used, mescaline was released and it had a longer duration in circulation, as compared to free mescaline.[7] The importance of the linker turns out to be clear for the use in the development of polymer-drug conjugates. The investigation in this research provides the path for the synthesis and characterization of

two polymer-drug conjugates, to be more precise a protein-drug conjugate and an antibody-drug conjugate. Both conjugates have the same drug, doxorubicin and the same linker, cobalt, the protein transferrin, and the antibody human immunoglobulin G. The synthesis of both conjugates occurred via cobalt coordination chemistry. The cobalt coordination chemistry took advantage of the amine group found in the doxorubicin molecule to crosslink it to the lysine residues in the polymers (see Figures 1 and 2).

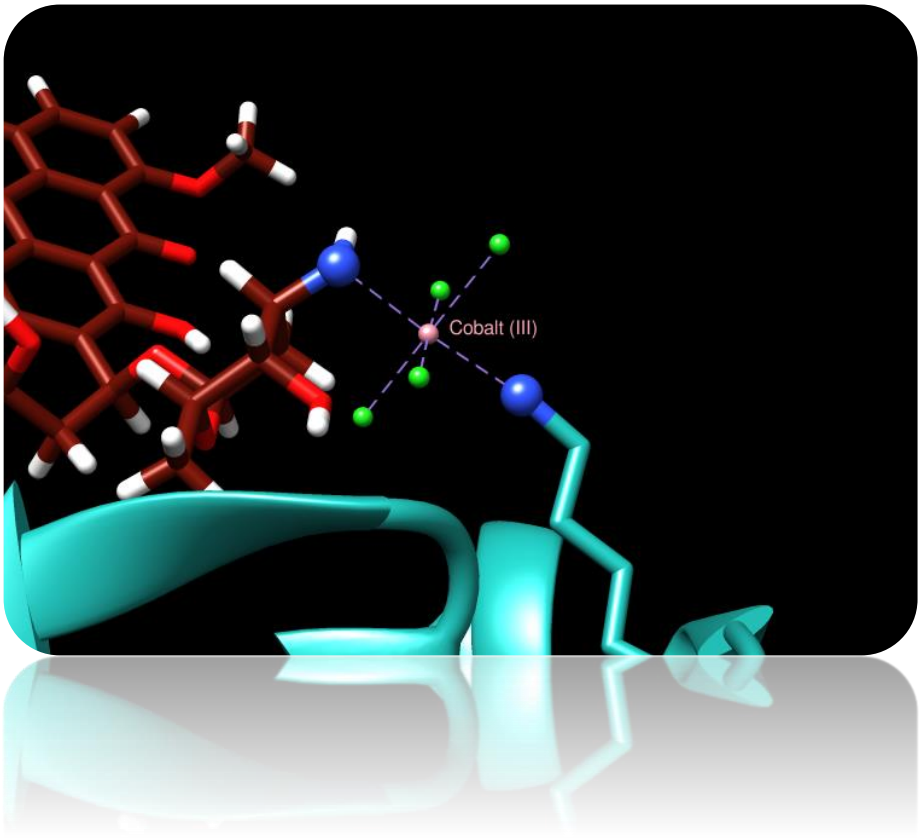

Figure 1. Illustration of the bonding between Dox and the protein via cobalt coordination chemistry.

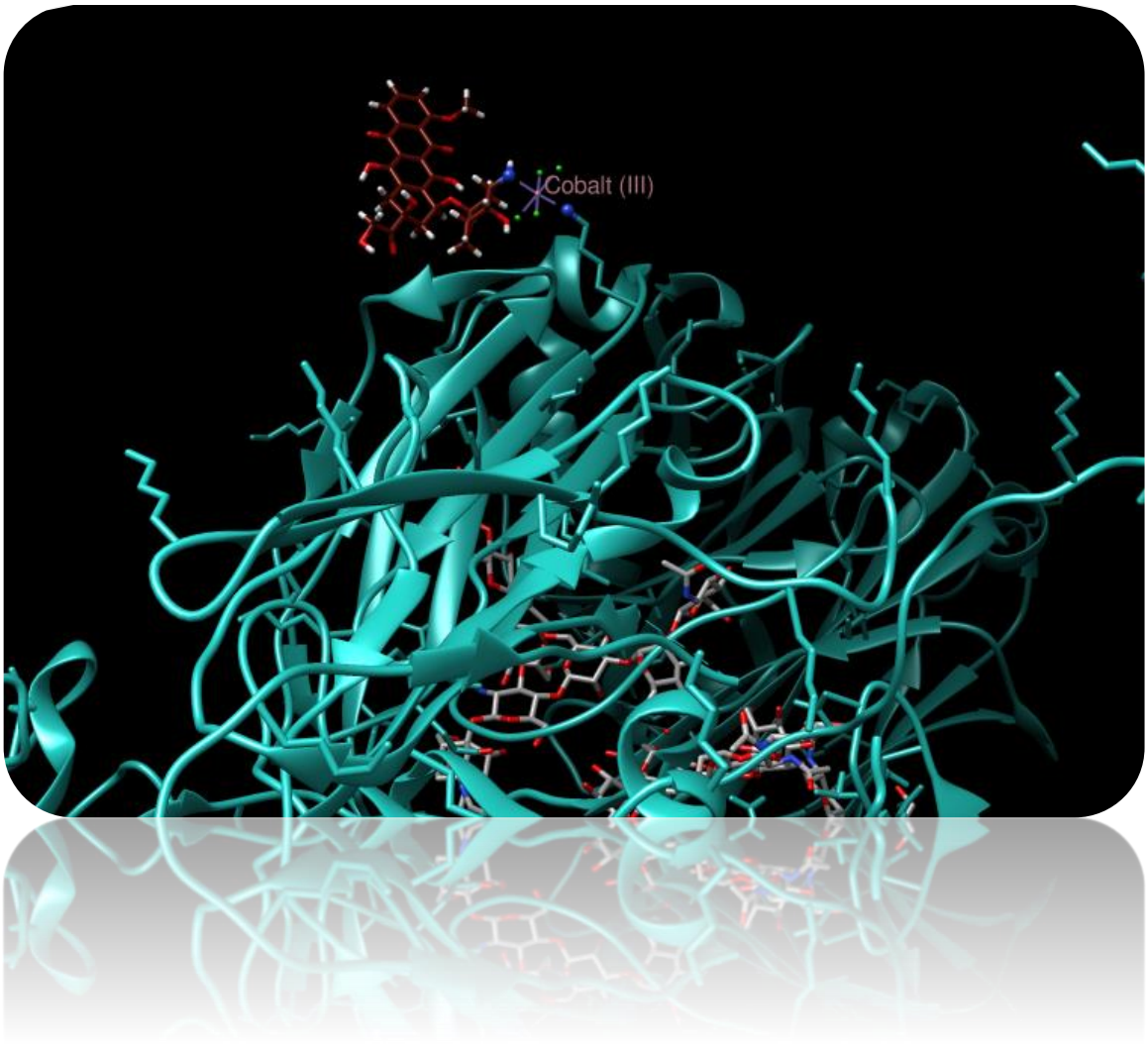

Figure 2. Illustration of the protein-Dox conjugate via cobalt coordination chemistry.

Doxorubicin (Adriamycin)

Doxorubicin (Dox; see Figure 3) was first isolated in 1967 from a mutant culture of *Streptomyces peucetius*, *Streptomyces peucetius caesius*.[10] Dox is an anthracycline antibiotic. Years before Dox another anthracycline was discovered, daunorubicin. Daunorubicin was the first anthracycline discovered to interact with tumor cells. Dox and

daunorubicin have extremely similar molecular structures, the only difference between the two is that the Dox primary chain ends with primary alcohol and the daunorubicin side chain ends with a methyl group. Doxorubicin is red in color at pH 7; an increase in pH causes the color to change to a violet blue color.[11] Dox is one of the most formidable chemotherapeutic agents available.[12] Dox can also be used to treat a wide variety of cancers. Dox causes its cytotoxic effect by intercalating into the DNA helix. The interaction causes the DNA to break and inhibits the synthesis of DNA and RNA. Dox is considered a poison for topoisomerase 2; the inhibition of this enzyme causes the breakage of the DNA double strand leading to apoptosis. Dox can form reactive oxygen species that can damage the DNA and cause cell death. Dox can obtain an electron by cellular NAD(P)H-oxidoreductases, leading to the formation of a semiquinone radical.[13] The semiquinone radical reacts with oxygen to produce superoxide and hydrogen peroxide, which are responsible for the DNA damage. Dox causes toxicity in the heart, brain, liver, and kidneys. The main concern when using Dox is the cardiotoxicity. The cause of the cardiac toxicity is not well understood.[12,14] A promising method to reduce the side effects caused by Dox is the use of a nanocarrier for an optimal delivery method. The small size of Dox makes it able to diffuse into healthy tissues, but by conjugating Dox to a polymer the diffusion will be prevented. As previously mentioned, tumor cells have a leaky vasculature, providing an opportunity for the Dox conjugate to accumulate near the cancer cells. For the conjugate to take optimal advantage of the EPR effect, the size of the polymer must be between 20 kDa to 200 kDa.[6]

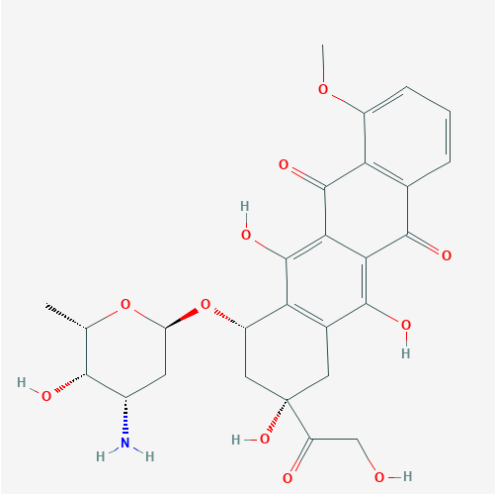

Figure 3. Chemical structure of doxorubicin.

Transferrin and Immunoglobulin G

Transferrin (Tf) is a glycoprotein found in blood plasma. Tf is made up of 678 amino acids, which account for two homologous lobes, and it has a molecular weight of 80 kDa.[15] The role of Tf is to transport iron to tissues by binding to the Tf receptor. Cancer cells overexpress the Tf receptor,[7–9] and it has been found the overexpression of the Tf receptor may be up to 100 times more in cancer cells than in regular cells.[16] The accessibility of the Tf receptor makes it an appealing target for drug delivery. Tf has more than 50 lysine residues. The conjugation number for Tf can vary; one study reports a conjugation number between 1 and 2[17], while another study reports a coordination number between 1 and 7.[18]

Immunoglobin G (IgG) is the most abundant antibody in the body. It consists of two light chains and two heavy chains, for a total molecular weight of 150 kDa. IgG has two antigen binding sites and a characteristic Y shape. There are four subclasses of IgG:

IgG1, IgG2, IgG3, and IgG4. IgG can function as a convenient carrier as it can target specific antigens only expressed or overexpressed by cancer cells.[19,20] IgG1 is widely use for the synthesis of conjugates, due to its secondary immune function.[19] There are only five approved antibody drug conjugates for therapeutic use.[20] IgG has approximately 90 lysine residues with about 30 lysine residues available for conjugation.[21] The conjugation number for IgG using lysine residues has been observed to be between 0 to 8.[21]

Cobalt as the Linker

The linker is an extremely important part, as it anchors the drug to the polymer. The linker must possess a set of unique properties. It needs to be stable in circulation, to prevent premature release of the drug, and the chemistry of the linker. The linker can be cleaved by three different methods. It can be cleaved by taking advantage of pH changes inside the cell, by enzymatic activity, or by a reducing environment.[19,20,22] Cobalt will be the linker for both polymer conjugates. Cobalt (Co) has low toxicity in the body.[23] The utilization of cobalt is based on Werner's theory and its ability to be reduced. Alfred Werner discovered that cobalt could interact with six ligands, not three, in an octahedral geometry. Co(III) complexes are usually inert, while Co(II) complexes are more labile. This due to Co(III) complexes having a low-spin, and Co(II) having a high-spin. The source of cobalt will be from cobalt (II) chloride hexahydrate ($CoCl_2 \cdot 6H_2O$). Previous experiments found $CoCl_2 \cdot 6H_2O$ as a suitable reagent to be used for prodrug synthesis.[22] The Co(II) can form bonds to the nitrogen group found in Dox and the nitrogen group from the lysine residues in IgG and Tf. The oxidation state of Co(II) can be changed to

Co(III) to create a more stable complex. The Co(III) complex can go reduction to Co(II) inside the tumor cell due to the high glutathione concentrations.[19,20,22,24] The reduction to Co(II) causes the release of Dox inside the cell.

Analytical Theories

Dialysis Cassette

Dialysis Cassette is a technique utilized for the separation of small molecules from samples based on diffusion. The dialysis cassettes contain a semi-permeable membrane with pores of a known size. The dialysis cassette is placed in a buffer solution where molecules smaller than the pore size will be able to freely diffuse out of the cassette. The dialysis cassettes come in different volumes and with different molecular weight cutoffs (MWCO). For this research, a dialysis cassette with a volume of 3 mL and a 3.5 K MWCO was used. The IgG has a molecular weight of 150 kDa, Tf has a molecular weight of 80 kDa, and Dox has a molecular weight of 543.5 Da. The only molecule able to diffuse through the membrane of the cassette was the unbound Dox. The dialysis cassette was utilized to determine the amount of Dox molecules conjugated to IgG, and Tf. It also helped determine the stability of the conjugates.

High Performance Liquid Chromatography

High Performance Liquid Chromatography (HPLC) is a technique for separation and identification of constituents where the mobile phase is a liquid. HPLC works under high pressures to reach reasonable flow rates. The stationary phase is the column. There are different types of columns with different properties. The type of the column and the

mobile phase will depend on the properties of the analyte. Dox is a hydrophobic molecule. Reverse phase liquid chromatography uses a non-polar column, and a polar solvent. This caused Dox to interact with the column and caused a longer retention time. The elution was isocratic, meaning it was a constant mobile phase composition. The mobile phase consisted of a mixture of 70% water and 30% acetonitrile. Acetonitrile was used to improve the solubility of Dox, as acetonitrile is less polar than water. The stationary phase consisted of an n-octadecyl (C18) column.

The HPLC to be used in these studies is equipped with a UV-Vis detector. The UV-Vis detector measures the absorbance of the solutes at a particular wavelength. Dox absorption spectra has peak maxima at 480 nm and 269 nm.[25] The UV-Vis spectra of Dox was determined using a UV-Vis spectrophotometer to further help with the development of the method. A UV-Vis instrument cannot be used for the quantification of Dox in the samples directly, because the absorption spectra of Co(II) has a peak maximum at around 480 nm.[26] The HPLC also has a fluorescence detector. The fluorescence spectra served as a second reference and matched the UV results.

Quasi-Elastic Light Scattering

Quasi-elastic light scattering (QELS) is also known as dynamic light scattering (DLS). The DLS technique measures the size of the particles, and it can identify aggregates in the solution. The measurement is performed by calculating the Doppler broadening of the Rayleigh-scattered light as a product of Brownian motion of the

particles. The identification of aggregates is important as they can cause immunogenic reactions among other problems.[27]

Cytotoxicity

The therapeutic effect on cells can be measured with a cytotoxic assay. The assay measured the toxicity of the conjugates in cancer cells. The therapeutic effect of the IgG-Dox conjugate and Tf-Dox conjugate was measured with 3-(4,5-dimethylthiazol-2-yl)-5-(3-carboxymethoxyphenyl)-2-(4-sulfophenyl)-2H-tetrazolium (MTS) assay. The MTS assay works by measuring the formazan product produced by cells. Only viable cells will be able to generate formazan from the reduction of the MTS tetrazolium compound. The absorbance of formazan was analyzed by a plate reader at a wavelength of 490 nm. The cell culture was MCF-7 cells, which is a human breast cancer cell line.

Differential Scanning Calorimetry

Differential Scanning Calorimetry (DSC) is a technique utilized for the determination of endothermic and exothermic process of biomolecules. DSC measures the heat flow and the temperature related with the thermal transitions. DSC operates by the thermal equivalent of ohm's law:

$$q = \frac{\Delta T}{R}$$

where "q stands for sample heat flow, ΔT is the temperature difference between the sample and reference, and R is the resistance of the thermoelectric disk".[28]

DSC instrumentation contains a reference cell and a sample cell. The temperature of both cells is changed identically. Since the sample cell contains the biomolecule, the

energy required to change the temperature in the sample cell is going to differ from the energy required to change the temperature in the reference cell. The difference in energy, therefore, is the heat absorbed or released by the biomolecule of interest.[28] The results can be further analyzed to determine the heat of denaturation of the biomolecule. The heat of denaturation of the Tf-Dox conjugate was compared to the heat of denaturation of the Tf protein to assure no denaturation happened during the synthesis of the conjugate. DSC study was only performed to the Tf-conjugate.

CHAPTER II

METHODOLOGY AND MATERIALS

Synthesis of Protein Drug Conjugates

The parameters for the synthesis of the IgG-Dox conjugate and Tf-Dox conjugate were obtained by synthesizing a Human Serum Albumin (HSA)-Dox conjugate. This was due to the limited amount of IgG and Tf, and the higher cost of IgG and Tf. Transferrin, Holo, Human Plasma (EDM Milipore Corp, Lot # 3139168), Human Immunoglobulin G Lyophilized Powder >= 97% (bioWorld, Lot# L18030603DV), Albumin, human crystallized (1x Cohn crystallized; MP Biomedicals, LLC Lot# Q2097), Dox HCL (Sigma Aldrich Lot# LRAB3692), Cobaltous Chloride Hexahydrate (Crystalline/Certified ACS, Fisher Chemical, Lot# 142533), 30% H_2O_2 solution, and NaOH (Reagent, ACS, GFS chemicals, Lot# P677895) were used for the conjugation reactions. Fresh solutions of 0.1 M $CoCl_2 \cdot 6H_2O$, and 0.25 M NaOH were prepared with ultrapure water before each experiment. Solutions of 5 $\frac{\text{mg}}{\text{mL}}$ Dox HCL were previously prepared by the research group and frozen for future use. An aliquot of the Dox HCL solution was thawed before each experiment.

The pH of various solutions was measured utilizing VWR symphony SB70P pH meter with an Orion 8103BN ROSS Combination Semi-micro pH Electrode. The pH meter was calibrated with stock pH buffer solutions of pH 2.0, pH 4.0, pH 7.0, and pH

10.0. The calibration of the pH meter was performed before the beginning of each experiment.

HSA-Dox Conjugate Parameters

Different Cobalt Oxidation Time

The synthesis of the HSA-Dox conjugate was performed by preparing a 10 $\frac{\text{mg}}{\text{mL}}$ solution of HSA in ultrapure water. Four aliquots of one mL were placed in glass vials. The pH of the HSA solution was increased by addition of a 0.25 M solution of NaOH. The increase of pH caused deprotonation of the lysine residues. The pH of the four HSA solutions was increased to 8.0. Four aliquots of 1 mL of ultrapure water were individually added into four different glass vials, followed by the addition of 200 μL of Dox HCl, 5 $\frac{\text{mg}}{\text{mL}}$, to each. The pH of the diluted Dox solution was increased to 8.0 using 0.25M NaOH; the solution changed color from a bright red to a darker red. The HSA solutions at pH 8.0 were added to the Dox solutions followed by the rapid addition of 52.5 μL of 0.1 M $CoCl_2 \cdot 6H_2O$ to all but one of the samples. Co(II) underwent ligand substitution with the free amine groups from the lysine residues and with the amine group from Dox. The reaction produced the HSA-Dox conjugate with Co(II) as the linker. As previously mentioned, Co(II) is a labile complex. Oxidation to Co(III) results in an exchange inert stable complex. Co(II) was oxidized after 24 hours by the addition of 2 μL of 30% H_2O_2 solution. The second vial was oxidized after 4 hours, and third vial after 10 min of adding the cobalt. The fourth vial did not contain any cobalt, nor H_2O_2. The samples were injected into dialysis cassettes after the addition of H_2O_2.

Change in pH

The synthesis of the HSA-Dox conjugate was performed by preparing a 10 $\frac{\text{mg}}{\text{mL}}$ solution of HSA with ultrapure water. Aliquots of 1 mL were place in six glass vials. The pH of the HSA solution was adjusted using 0.25 M NaOH. Two vials were increased to a pH of 8.5, two to a pH of 9.0, and the last two to a pH of 9.5. Aliquots of one mL of ultrapure water were individually added into six different glass vials followed by the addition of 200 μL of Dox HCl, 5 $\frac{\text{mg}}{\text{mL}}$, to each vial. The pH of the diluted Dox solutions was adjusted to a pH of 8.5 using 0.25M NaOH. The solution changed color from a bright red to a darker red for pH 8.5 and a dark violet for pH 9.5. The HSA solution with pH 8.5 was added to the Dox solution pH 8.5 followed by the rapid addition of 52.5 μL of 0.1 M $CoCl_2 \cdot 6H_2O$. Co(II) was oxidized after 24 hours with the addition of 2 μL of 30% H_2O_2. The same steps were repeated for one solution of HSA at pH of 9.0, and one at pH of 9.5 The other three HSA solutions with pH 8.5, pH 9.0, and 9.5 were prepared exactly the same except without the addition of cobalt. After 24 hours, and the addition of H_2O_2 to the samples containing cobalt, the samples were injected into dialysis cassettes.

Change in Cobalt Concentration

The synthesis of the HSA-Dox conjugates was performed by preparing a 10 $\frac{\text{mg}}{\text{mL}}$ solution of HSA with ultrapure water. Aliquots of one mL were place in five different glass vials. The pH of the HSA solutions was adjusted to a pH of 8.5 using 0.25 M NaOH. Aliquots of one mL of ultrapure water were individually added into five different

glass vials followed by the addition of 200 μL of Dox HCl, 5 $\frac{mg}{mL}$, to each vial. The pH of the diluted Dox solutions was adjusted to a pH of 8.5 using 0.25 M NaOH. The solutions change color from a bright red to a darker red. One of the pH adjusted HSA solutions was added to one of the Dox solutions followed by the rapid addition of 26 μL of 0.1 M $CoCl_2 \cdot 6H_2O$. The same procedure was repeated for Vials 2, 3, 4, and 5, with the variation of different $CoCl_2 \cdot 6H_2O$ volumes. For Vial 2, 52.5 μL of 0.1 M $CoCl_2 \cdot 6H_2O$ was added. For Vial 3, 78.5 μL of 0.1 M $CoCl_2 \cdot 6H_2O$ was added. For Vial 4, 105 μL of 0.1 M $CoCl_2 \cdot 6H_2O$ was added. Co(II) was oxidized after 24 hours through the addition of 2 μL of 30% H_2O_2 into each vial. The fifth vial did not contain any cobalt, or H_2O_2. The samples were injected into dialysis cassettes after the addition of H_2O_2.

Change in Dox Concentration

The synthesis of the HSA-Dox conjugates was performed by preparing a 10 $\frac{mg}{mL}$ solution of HSA with ultrapure water. Four aliquots of 1 mL were place in four different glass vials, 1 mL per vial. The pH of the HSA solution was increased by micro additions of 0.25 M solution of NaOH. The increase of pH caused deprotonation of the lysine residues. The pH of the HSA solutions was increased to a pH of 8.5. Four aliquots of 1 mL of ultrapure water were individually added into four different glass vials, 1 mL per vial followed by the addition of 50 μL of Dox HCl, 5 $\frac{mg}{mL}$, in Vial 1. One hundred microliters of Dox HCl, 5 $\frac{mg}{mL}$, were added to Vial 2. Two hundred microliters of Dox HCl, 5 $\frac{mg}{mL}$, were added to vial 3. Four hundred microliters of Dox HCl, 5 $\frac{mg}{mL}$, were added

to Vial 4. The pH of the diluted Dox solution was increased to a pH of 8.5 by the micro addition of the 0.25M NaOH solution. The HSA solution with pH 8.5 was added to the Dox solution in Vial 1 followed by the rapid addition of 52.5 μL of $CoCl_2 \cdot 6H_2O$. The same HSA addition to the Dox was repeated for Vial 2, 3, and 4. Co(II) was oxidized after 24 hours with the addition of 2 μL of 30% H_2O_2 into each vial. The samples were injected into dialysis cassettes after the addition of H_2O_2.

Tf-Dox Conjugate and IgG-Dox conjugate

Synthesis of Tf-Dox Conjugate

The synthesis of the Tf-Dox conjugate was performed by preparing a 10 $\frac{\text{mg}}{\text{mL}}$ solution of Tf in ultrapure water. One milliliter of the Tf solution was place in a glass vial. The pH of the Tf solution was increased by micro additions of 0.25 M solution of NaOH, causing deprotonation of the nitrogen of lysine residues. The pH of the Tf solution was increased to 8.5. One milliliter of ultrapure water was added into a different glass vial, followed by the addition of 200 μL of Dox HCl, 5 $\frac{\text{mg}}{\text{mL}}$. The pH of the diluted Dox solution was increased to 8.5 by the micro addition of the 0.25M NaOH solution; the solution changed color from a bright red to a darker red. The Tf solution at pH 8.5 was added to the Dox solution followed by the rapid addition of 52.5 μL of 0.1 M $CoCl_2 \cdot 6H_2O$ at which time the solution color changed to a dark violet. Co(II) was oxidized after 24 hours through the addition of 2 μL of 30% H_2O_2. The conjugate was injected into dialysis cassette after the addition of H_2O_2.

Synthesis of IgG-Dox Conjugate

The synthesis of the IgG-Dox conjugate was performed by preparing a 10 $\frac{\text{mg}}{\text{mL}}$ solution of IgG in ultrapure water. One milliliter of the IgG solution was placed in a glass vial. The pH of the IgG solution was increased by micro additions of 0.25 M solution of NaOH, causing the deprotonation of the nitrogen of the lysine residues. The pH of the IgG solution was increased to 8.5. One milliliter of ultrapure water was added into a different glass vial, followed by the addition of 200 μL of Dox HCl, 5 $\frac{\text{mg}}{\text{mL}}$. The pH of the diluted Dox solution was increased to a pH of 8.5 by the micro addition of the 0.25M NaOH solution, which resulted in the solution changing color from a bright red to a darker red. The IgG solution at pH 8.5 was added to the Dox solution followed by the rapid addition of 52.5 μL of $CoCl_2 \cdot 6H_2O$ at which time the solution changed color to a dark violet. Co(II) was oxidized after 24 hours through the addition of 2 μL of 30% H_2O_2. The conjugate was injected into dialysis cassette after the addition of H_2O_2.

Characterization of the Conjugates

The characterization of the newly synthesized conjugates was performed using dialysis cassettes, and HPLC. DSC was used to analyze the stability and DLS was used to measure the size and check for protein aggregation. Cytotoxicity was measured via an MTS assay in a human breast cancer cell line (MCF-7 cells).

Calibration Standards

A solution containing only Dox was prepared in order to generate a calibration curve. The calibration curve of this standardized Dox solution was used to quantify the

amount of Dox in unknown samples and ultimately to determine the number of Dox molecules conjugated per protein. The Dox-only sample was prepared by adding 2 mL of ultrapure water in a glass vial with 200 μL of Dox HCl, 5 $\frac{\text{mg}}{\text{mL}}$. The pH of the Dox solution was increased to match the pH of the conjugate solution, but due to solubility issues encountered on the first set of experiments, the pH for this solution was not adjusted for the subsequent experiments. The Dox-only solution was prepared in conjunction with each set of experiments. The Dox-only solution was then injected into a dialysis cassette.

Dialysis Cassette

A solution of 1X phosphate buffered saline (PBS) was prepared by mixing one part 10X PBS (Fischer Bioreagents Lot# 153384) with nine parts of ultrapure water. The conjugates were injected with a 5 mL disposable syringe (Excelint Lot# 141004) into dialysis cassettes (3,500 MWCO, 0.2–3 mL sample capacity, Slide-A-Lyzer Lot# LE144493). The dialysis cassettes were immersed in ultrapure water for 1 minute per side prior to adding the samples. Each cassette was immersed in a beaker filled with 200 mL of 1X PBS. A separate cassette was loaded with the Dox-only solution and it was immersed in a separate beaker filled with 200 mL of 1X PBS. The cassettes were incubated for 72 hr. During the incubation period unbound Dox was able to diffuse out of the cassette into the 1X PBS bulk phase. This was observed by a change of color of the 1X PBS from clear to a transparent orange color. Three dilutions were made from the bulk solution from Dox-only sample, 1:3, 1:6, and 1:10. The dilutions were made by diluting the bulk solution with the stock solution of 1X PBS. A sample of 1.5 mL 1X

PBS, the bulk solution, was placed in a HPLC autosampler vial (2 mL screw glass vial, Agilent) for further analysis, as well as the dilutions from the Dox bulk solution. The sample in the cassette was removed and refrigerated in a 2 mL micro centrifuge tube for further analysis.

HPLC

The HPLC used was an Agilent 1220 Infinity II LC with configuration G4290B and fluorescence detector G7121A. The components of the configuration were dual-channel gradient pump (with degasser), autosampler, column oven, and variable wavelength detector. HPLC was used to separate Dox from cobalt to prevent any error of identification and quantification. The HPLC vials (Agilent Technologies) with the sample collected from the bulk solution were labeled and placed in the autosampler tray. The analysis was performed using Agilent OpenLAB ChemStation software. The area under the curve of the Dox peak is directly proportional to its concentration. The concentration of Dox in the conjugates was calculated by analyzing the known concentration in the sample of Dox-only. A series of dilutions from the Dox-only sample were used to create a calibration curve. A sample of 1X PBS only was also analyzed. The number of Dox molecules/protein was calculated once the concentrations of the unknown bulk phases were obtained from the slope equation of the calibration curve. Calculations were performed in an Excel spread sheet.

HPLC Method

The method used for the HPLC analysis was created based on previous work from the research group. The solvent consisted of a 70:30 mixture of ultrapure water with HPLC grade acetonitrile (≥ 99.9%, HiPerSolv CHROMANORM, VWR Chemicals). The ultrapure water was acidified to a pH 3.0, before mixing with acetonitrile, by the micro addition of o-phosphoric acid (85% W/W, Millipore Sigma). The column used was a Shimadzu Premier C18 column (5 micron, 4.6 x 150mm). The elution was isocratic with a flow rate of 1.000 mL/min and resulted in a pressure of ~128 bar. The injection volume was set to 20 μL and the stop time to 9 min. The fluorescence excitation wavelength was set to 542 nm and the emission wavelength was set to 600 nm. The excitation and emission wavelengths were determined by analyzing sample of Dox in a spectrofluorophotometer (Shimadzu RF-5301PC). The spectrofluorophotometer had the option to find the optimal wavelengths. The UV-Vis wavelength used was 233 nm. The UV-Vis wavelength was determined using a Shimadzu UV-2401PC. The spectra of a Dox sample was collected by scanning from 190 nm to 800 nm. A sample of dox was analyzed by HPLC using different wavelengths, 233 nm, 253 nm, 290 nm, and 480 nm. Each sample was run in triplicates.

QELS or DLS

The size of the conjugates was measured using Microtrac MRB's NANOTRAC Wave II with a Teflon sample cell. The data from the scans was analyzed with Microtrac FLEX software. The conjugate samples were loaded in the cell using a 5 mL plastic

transfer pipette (VWR Chemicals, Lot# 03022020). The loading index for all the conjugates was above 0.1. The cell was cleaned after each sample by filling it with ultrapure water and brushing it with a cleaning swab (TX710A, Texwipe). The sample cell was rinsed once again with ultrapure water and the loading index was checked with ultrapure water to make sure it was below 0.01. There were a total of six runs of 30 second each per sample. The average of the six runs was calculated by the Microtrac FLEX software.

DSC

The DSC used was a Nano DSC by TA instruments. The 1X PBS, Tf-Dox conjugate, and Tf protein solutions were degas (Degassing Station by TA instruments) for 15 min at 400 mmHg. The samples were loaded by utilizing the method described in the user's manual. A baseline was created by doing a heating run of 1X PBS vs 1X PBS at a scan rate of 1 ºC/min from 25 ºC to 115 ºC at a pressure of 3 atm and equilibration time of 600 seconds. Solutions of 1 $\frac{mg}{mL}$ Tf and 1 $\frac{mg}{mL}$ Tf-Dox conjugate were prepared by diluting stock solutions in 1X PBS. The Tf protein and Tf-Dox conjugate were analyzed using the same parameters. The instrument was cleaned after each run with 100 mL 2% solution of Cole-Parmer® Micro-90 Cleaning Solution and rinsed with 600 mL of ultrapure water. The data was analyzed with DSCRun software.

Cytotoxicity

Cell experiments were performed using aseptic technique to prevent any contamination of the cell culture. The cell line was MCF-7 cells, which were provided by

Dr. Bergel's group from the biology department at Texas Woman's University. A 70% ethanol solution was used to clean all lab equipment and workstations. Cell culture was performed inside a laminar flow hood sterilized by UV light. The cell cultures were stored in an incubator and maintained every other day. They were incubated at 37 ºC with 5% CO_2 in Dulbecco's Modified Eagle's medium (DMEM; Gibco) . DMEM provides the nutrients to support the growth of the cells. The cells were trypsinized to collect a sample to use in the MTS assay (ab197010, abcam). A sample of 100 µL cell suspension was transferred to an Eppendorf tube and mixed with 100 µL of Trypan Blue. Ten microliters were added to each side of the hemocytometer. Cells in the four corner squares and middle square were counted via microscopy. Based on the cell count, calculations were performed to achieve solutions containing cell concentrations resulting in 10,000 cells per well in a 96-well plate (Flat Clear Bottom Black Polystyrene TC-treated Microplates, Corning). The wells were filled with a total volume of 95 µL cell suspension and the plate was incubated for 1 day. The following day, 5 µL of the IgG-Dox conjugate, Tf-Dox conjugate, HSA-Dox conjugate, and Dox were added to different rows of the plate. Each row was labeled for identification and the plate was incubated for 72 hours. After incubation, the wells were aspirated to prevent any interference from the absorbance of Dox because it has an absorbance overlapping the region containing the formazan product peak. After aspirating, the MTS Assay was performed by mixing the MTS reagent with DMEM and adding 105 µL to each well. The plate was incubated for an additional hour and then analyzed utilizing a microplate reader (BioTek Synergy H1).

CHAPTER III

RESULTS

Synthesis and Characterization of Protein-Dox Conjugates

HPLC Studies

The number of Dox molecules/protein for each set of reaction conditions was calculated by calculating the area under the curve of the Dox peak obtained via HPLC analysis. Most results were as expected, with exception of a few samples that are discussed below.

Different Cobalt Oxidation Times

The effects of the cobalt oxidation time were first studied to the impact of reaction time to the number of Dox molecules/protein. The oxidation times were 10 minutes, 4 hours, and 24 hours. It was found that the oxidation time did not impact the conjugation efficiency. Due to an issue with the calibration sample of Dox, the number of Dox molecules/protein was not calculated for this set of experiments. The issue is discussed later in this thesis. The average area under the curve for the three samples analyzed were 79.9 for 10 min, 79.7 for 4 hours, and 80.0 for 24 hours (see Figure 4, Table 1). Based on these results, it was apparent that the oxidation time of cobalt did not change the number of Dox molecules attached to the protein. The calibration sample of Dox had a smaller average area (see Table 2), 62.2, than the samples which made the quantification of the number of Dox molecules/protein unattainable. All samples were expected to be smaller

in area compared to the Dox-only sample because 100% of the Dox should have been released into the bulk phase. The UV wavelength monitored for this experiment was 253 nm, and the fluorescence signal was not monitored. The parameters were examined in an effort to generate a more robust method for the next set of experiments and to determine the source of peaks eluting at 1.5 min, and 2 minutes.

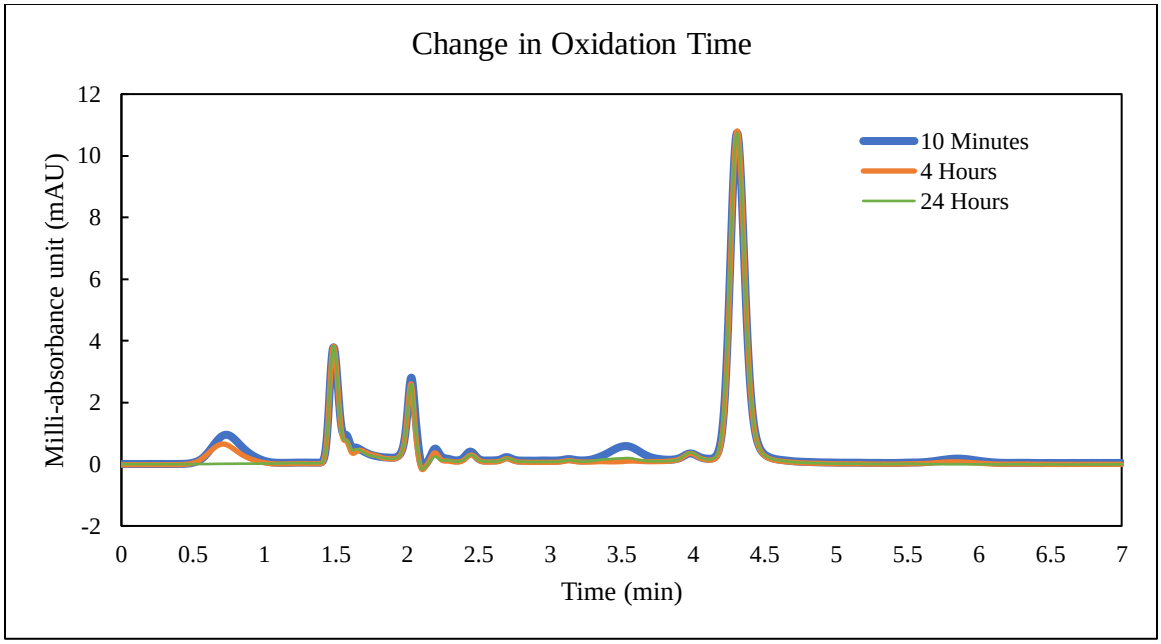

Figure 4. HPLC absorbance chromatograms of cobalt oxidation time at 10 minutes, 4 hours, and 24 hours.

Table 1. HPLC Results from the Change In Oxidation Time

	10 Minutes	4 hours	24 hours
Area 1	80.0	79.9	80.3
Area 2	80.1	79.8	80.1
Area 3	79.6	79.5	79.6
Average Area	79.9	79.7	80.0

Table 2. HPLC Results from the Calibration Curve

	DOX Undiluted	1:3	1:6	1:10
Area 1	62.5	20.3	8.0	4.8
Area 2	62.4	20.2	8.5	4.9
Area 3	61.6	20.1	8.0	4.7
Average Area	62.2	20.2	8.2	4.8

The Dox-only control sample was used to create a calibration curve (see Figure 5) for the quantification of Dox in each of the samples. The cassette injected with Dox-only served as a reference amount of how much Dox can theoretically accumulate in the bulk phase. Again, the bulk phase for the Dox-only control was expected to have a higher Dox concentration because Dox can freely diffuse through the membrane because of its size and because it is not bound to something larger. This assumption was found to be incorrect for the first sample; however, a better method was developed that worked better in future experiments. The analyte of interest was Dox which gives rise to the peak observed at 4.3 minutes. The peak at 4.3 min in the chromatograms of bulk phase increased in magnitude as the concentration of Dox increased, while the peaks at 1.5 and 2 min remained constant (see Figure 6).

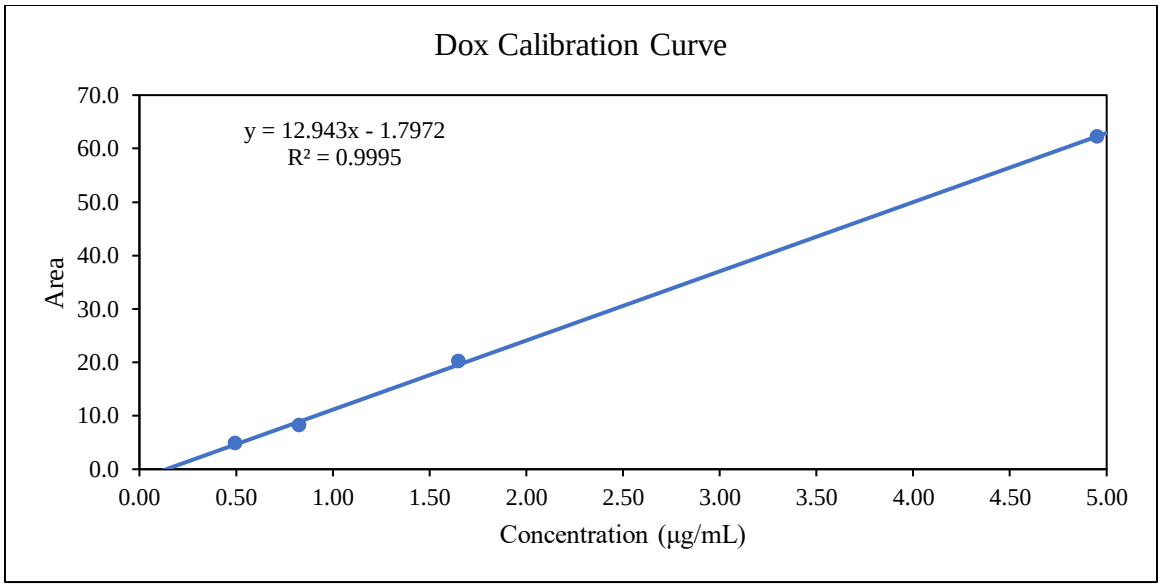

Figure 5. Calibration curve based on the bulk sample.

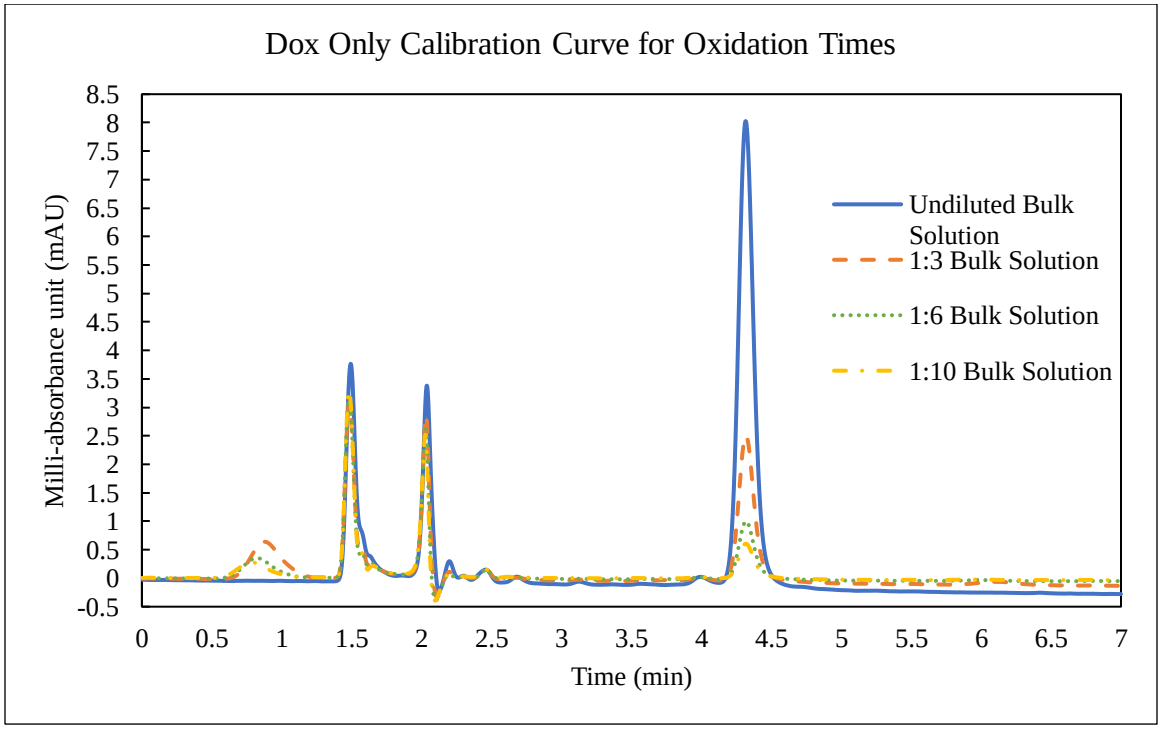

Figure 6. HPLC absorbance chromatograms of dilutions of the bulk sample.

The highest concentration of Dox in the bulk phase was calculated to be 4.95 $\frac{\mu g}{mL}$, by using:

$$C_1V_1 = C_2V_2 \rightarrow C_2 = \frac{C_1V_1}{V_2}$$

Where C_1 was the initial concentration, V_1 was the initial volume, C_2 the final concentration, and V_2 the final volume. The initial concentration was 5000 $\frac{\mu g}{mL}$, the initial volume was 0.2 mL, and the final volume was 202 mL.

UV-Vis and Fluorescence Wavelengths

The UV-Vis spectrum of dox was collected in order to determine maximum absorbance and emission wavelengths in an effort to create a more robust analytical method. The UV-Vis spectrum of Dox had absorbance peaks centered at 192 nm, 233 nm, 253 nm, 289 nm, and 481 nm (see Figure 7). The UV-Vis spectrum of 1X PBS had an absorption peak centered at 192 nm (see Figure 8). The solution of Dox in 1X PBS and acetonitrile caused an increase in the absorbance at 197 nm, and a slight increase in the absorbance at 253 nm.

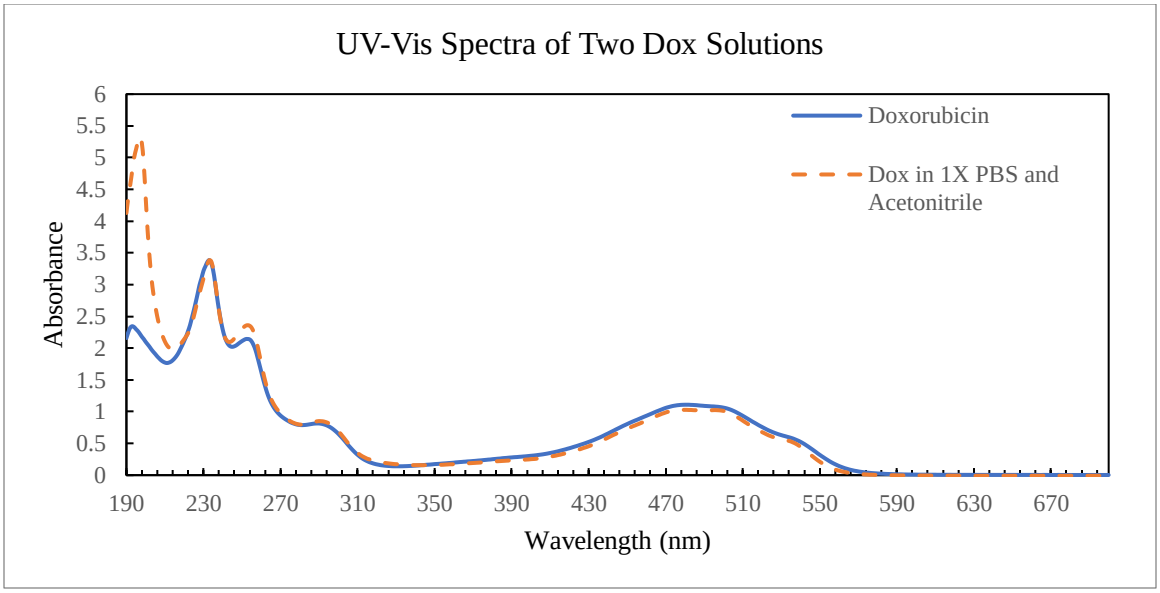

Figure 7. Absorbance spectra of Dox and Dox in 1X PBS with Acetonitrile.

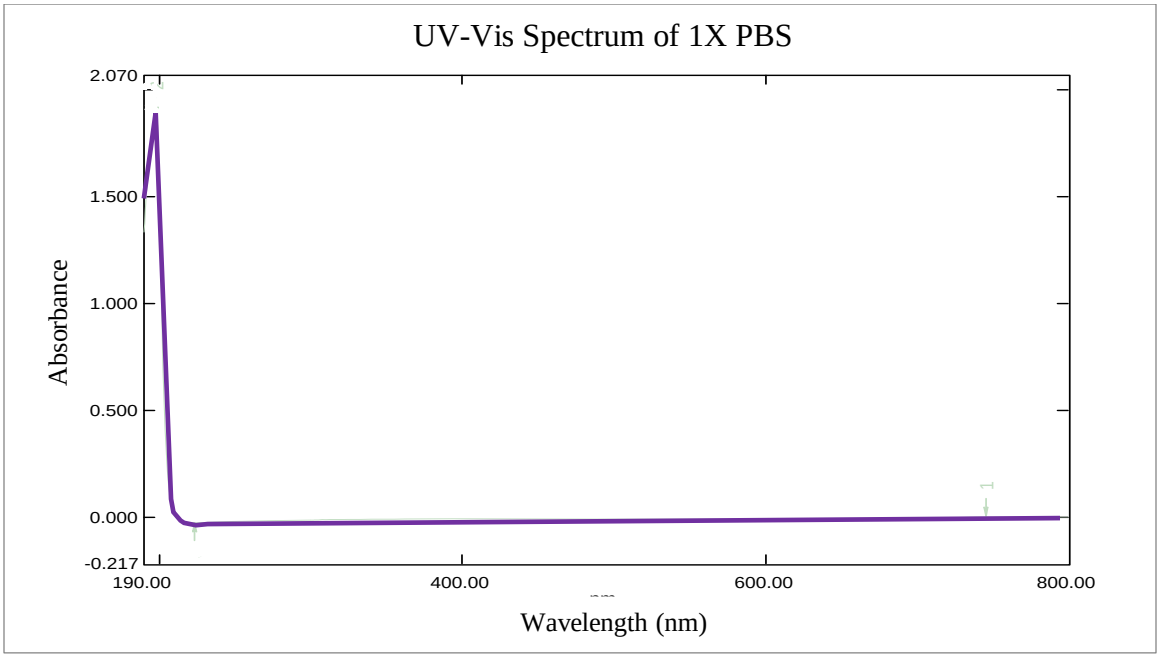

Figure 8. Absorbance spectrum of 1X PBS.

The maximum absorbance in HPLC was observed at 233 nm for Dox in 1X PBS (see Figure 9). Due to the overlap of absorbances of cobalt and PBS wavelengths of 192 nm and 480 nm were not considered for use.

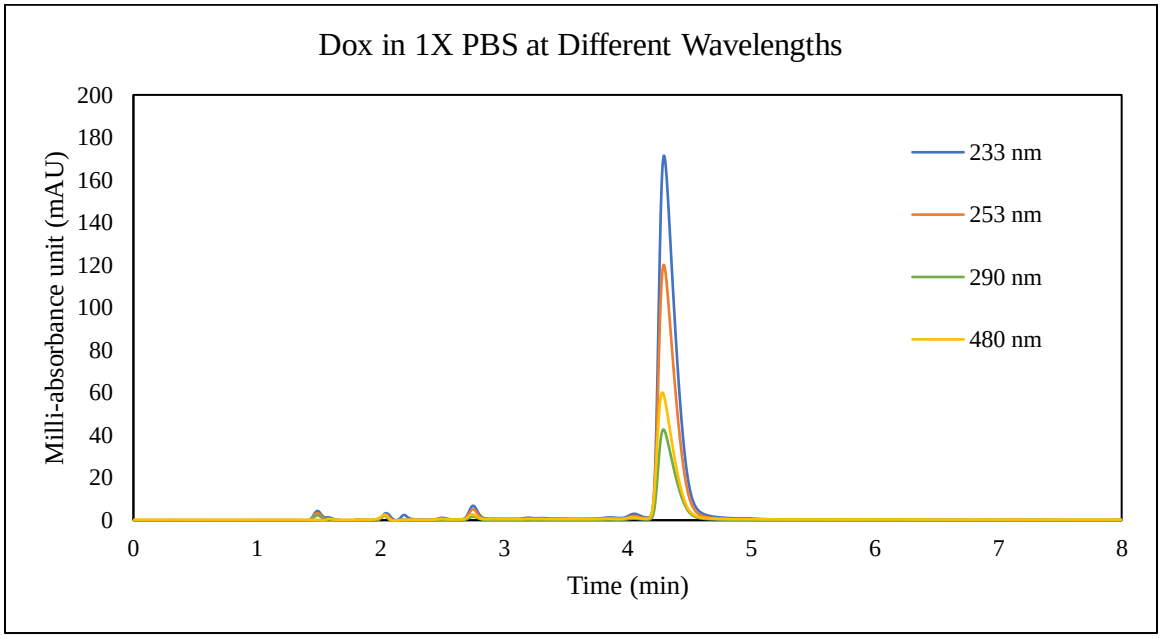

Figure 9. HPLC absorbance chromatograms of Dox in 1X PBS at different wavelengths.

The HPLC results of Dox in 1X PBS also contained some unidentified peaks during the first 3 minutes of the run time. These peaks were confirmed to come from the 1X PBS solution by running two samples of 1X PBS (see Figure 10). The chromatogram contained peaks at the same retention time albeit with a slight variation of the intensity (see Figure 11).

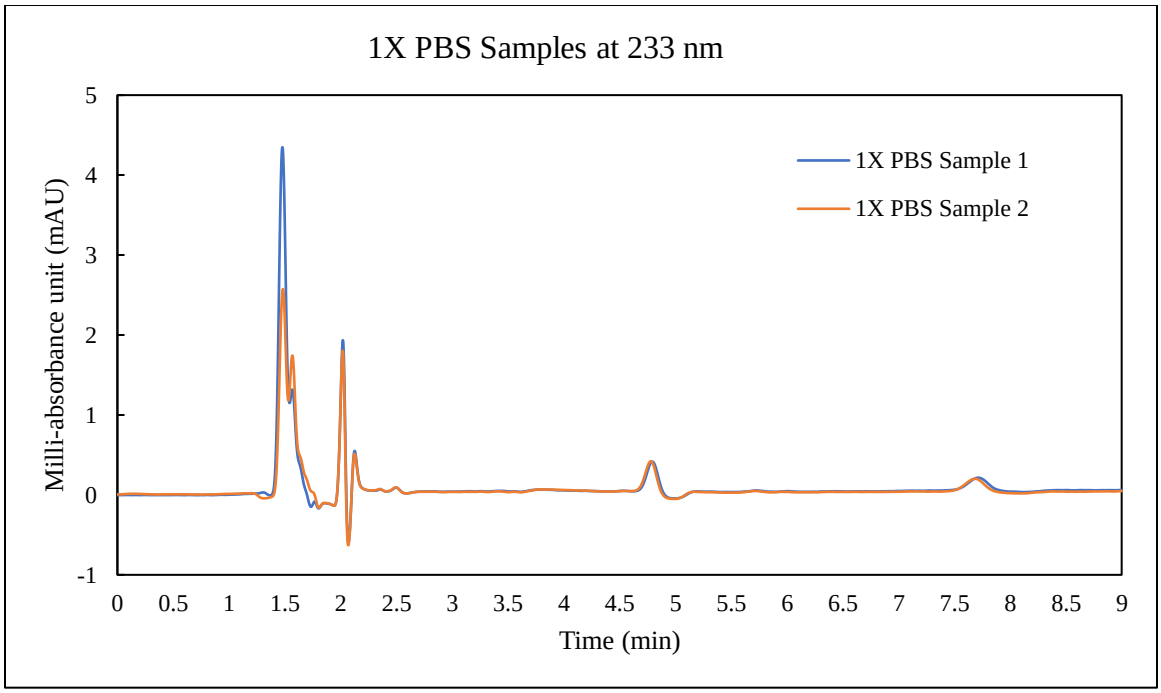

Figure 10. HPLC absorbance chromatograms of 1X PBS Samples at 233 nm.

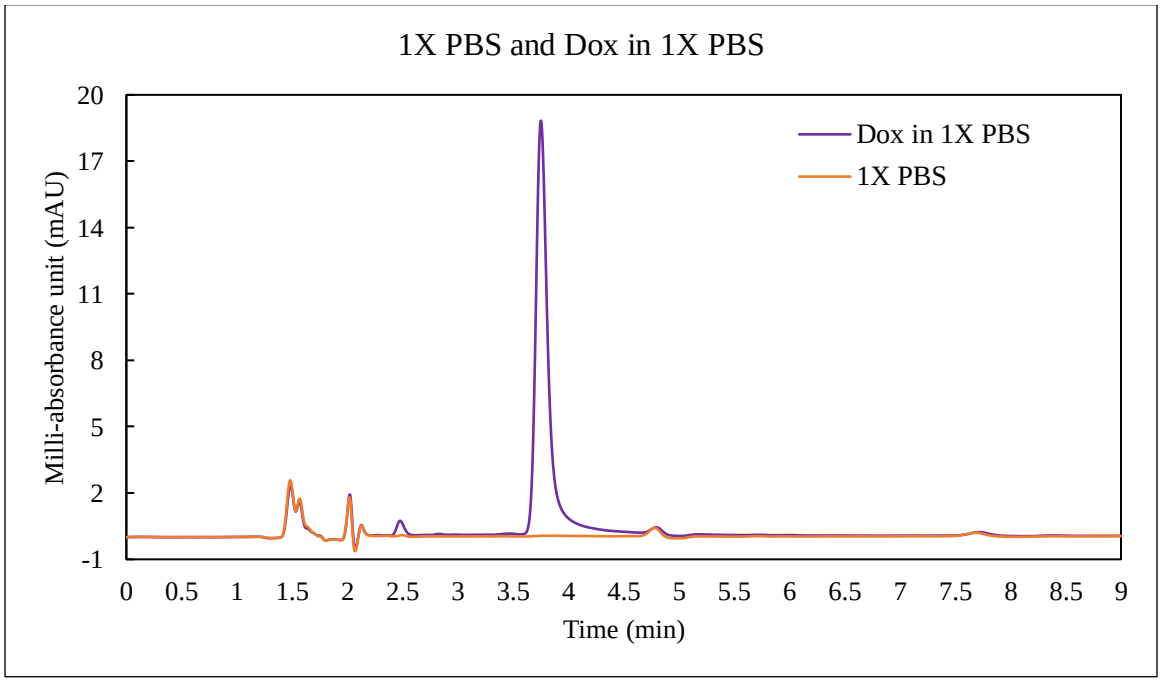

Figure 11. HPLC absorbance chromatograms of 1X PBS and Dox in 1X PBS.

An experiment performed with the spectrofluorometer was used to determine the optimal excitation/emission wavelengths for Dox, which were found to be 542 nm for excitation and 600 nm for emission. When monitoring the HPLC via the fluorescence detector, a peak at the expected retention time for Dox was observed (see Figure 12). No peaks were observed for PBS as expected since it does not fluoresce (see Figure 13). The advantage of using the fluorescence detector was the absence of peaks due to 1X PBS, which helped to reduce identification and quantification errors.

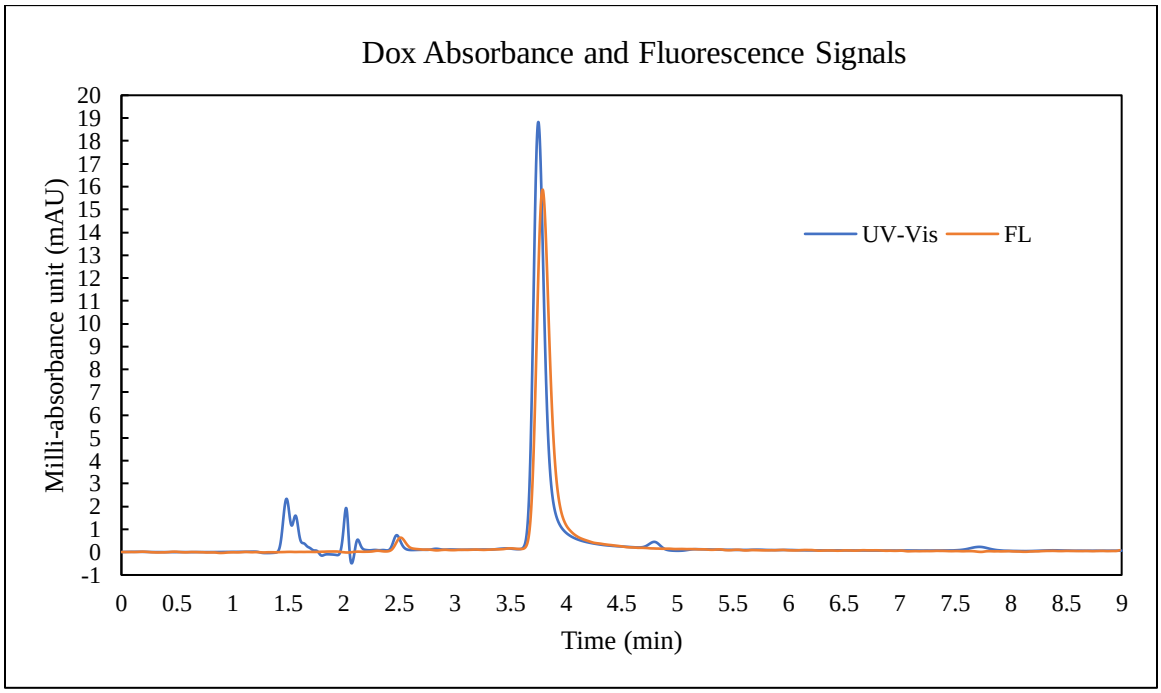

Figure 12. HPLC chromatograms of absorbance signal and fluorescence signal from Dox at the same scale.

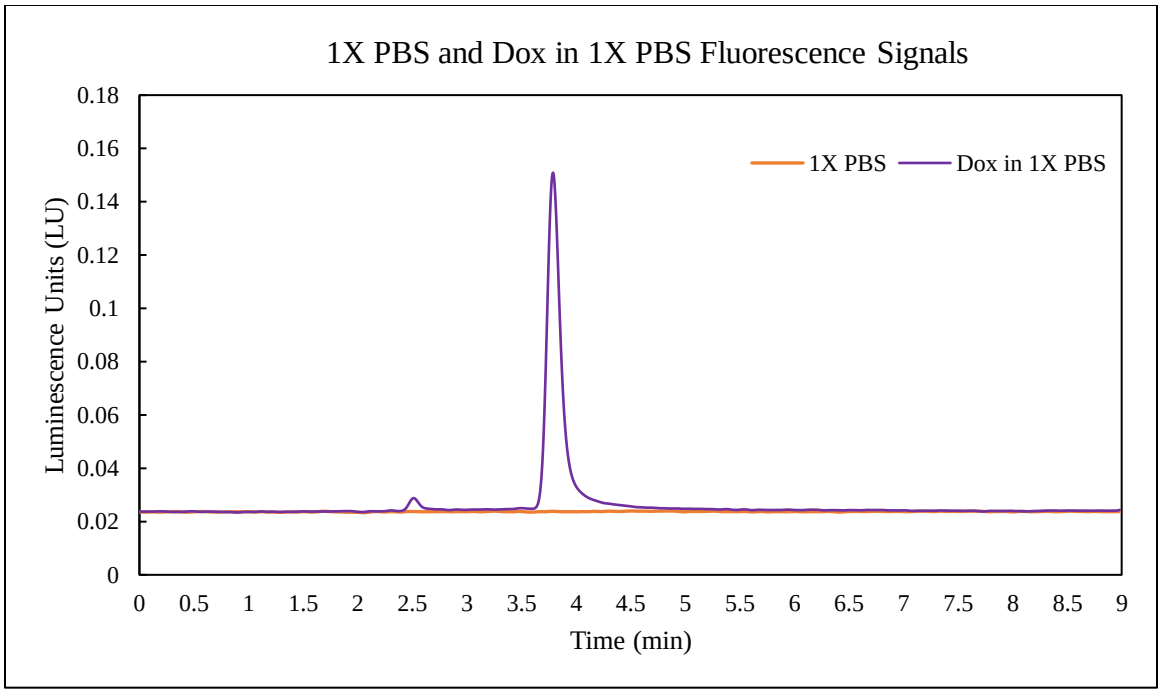

Figure 13. HPLC chromatograms of fluorescence signals from 1X PBS and Dox in 1X PBS.

Based on the results obtained in these experiments, the method was modified to use these wavelengths for all future experiments aimed at characterizing the conjugates.

Change in pH

Different pH were tested to observe the effect to the amount of Dox conjugated to the protein. The increase in pH should cause more deprotonation of the nitrogen group in the lysine residues and the nitrogen group in Dox. It was expected to observe higher conjugation efficiency with increasing pH. Two sets of solutions were tested, one set with cobalt and the other set without cobalt. The set without cobalt was expected to have a lower conjugation number due to no conjugation at all since the linker, cobalt, was not present.

The first trial of the experiment gave unexpected results. The samples without cobalt retained more Dox inside the cassette. The bulk phase of the samples with cobalt had a more intense red-orange color (see Figure 14). The higher tint indicates a higher concentration of Dox in the bulk phase, therefore less Dox molecules bound to HSA.

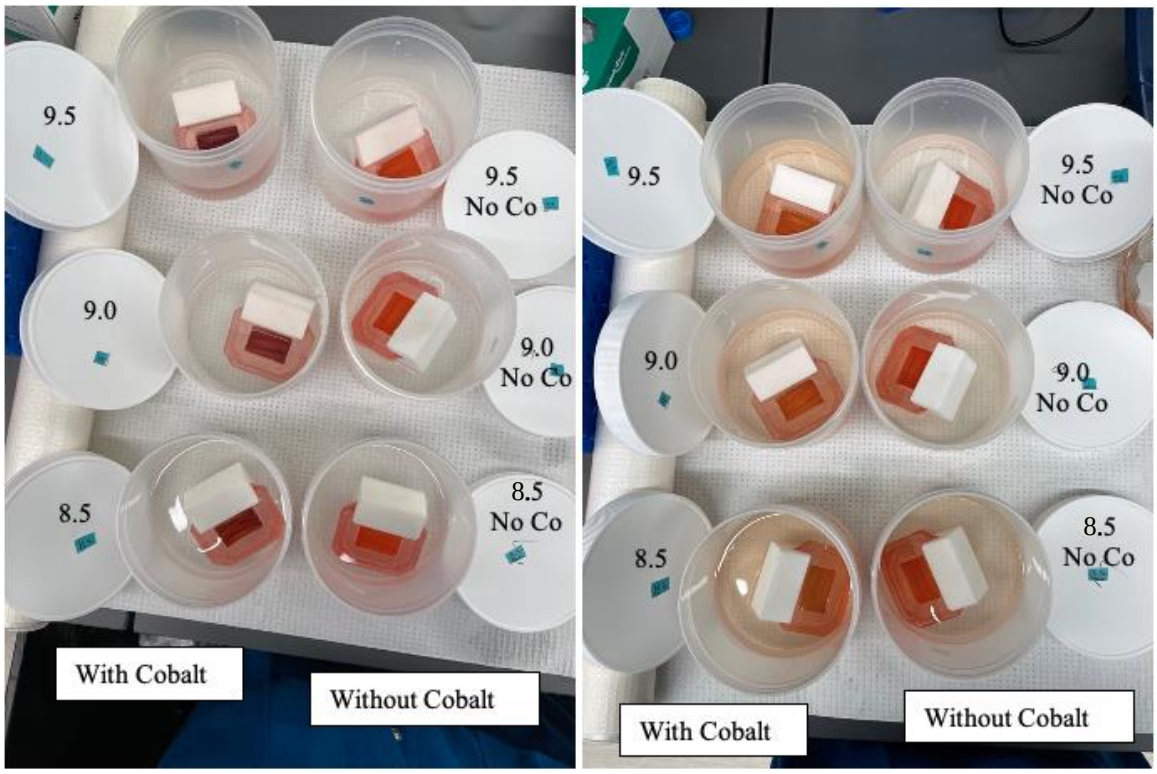

Figure 14. Different pH samples before and after. The left picture is the initial set up of the experiment. The right picture is after 72 hours. The bulk sample of the samples with cobalt after 72 hours had a higher red tint than the samples without cobalt. This indicates a higher release of Dox, which means a lower conjugation number.

The samples were left undisturbed for a total of 10 days, to see if any more Dox would diffuse out of the cassettes. The difference inside the cassettes after 10 days was readily observable. The cassettes containing no cobalt formed into what appeared to be a red rectangular precipitate, while the samples with cobalt did not form similar structures

(see Figure 15). The samples with cobalt appeared to have small amounts of precipitate. Due to the fact that virtually no Dox was released in the control samples no HPLC studies were performed.

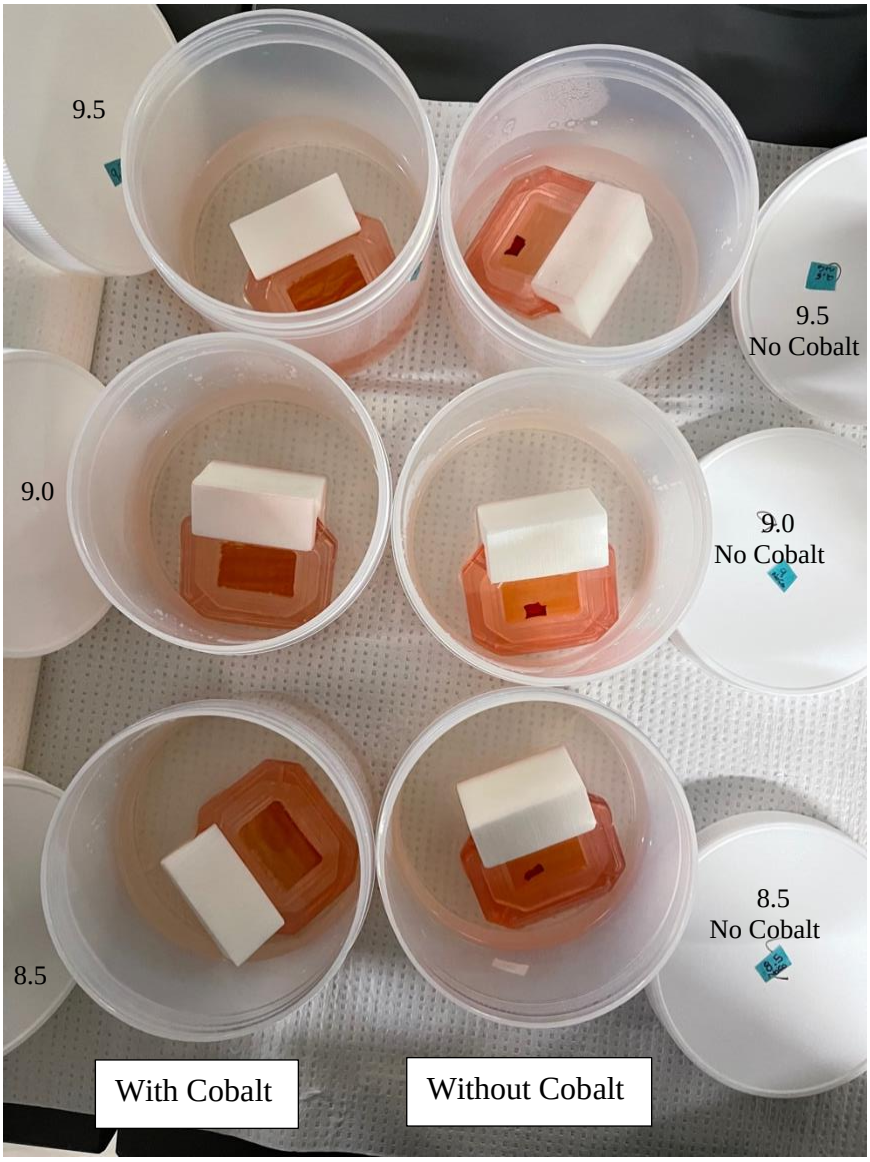

Figure 15. Different pH samples after 10 days.

The experiment was repeated a second time, but as soon as the pH of the Dox solution was changed the HSA and cobalt were added. In the first trial the pH of Dox was changed and the Dox solution was allowed to sit on the bench while the pH of the HSA was adjusted. The results from the second trial were more in line with expectation except for the solution of pH 8.5 with cobalt. The solutions with cobalt followed the trend of the higher the pH the higher the conjugation efficiency, and the solutions without cobalt released more Dox than the solutions with cobalt.

Both signals' peaks were at roughly 3.7 minutes (the solution travels through the absorbance detector first; see Figures 16 and 17). The absorbance peaks attributed to PBS were present for all samples with no change in the amplitude. The results obtained from the fluorescence signals matched the results obtained from the absorbance signals for each sample (see Figure 18).

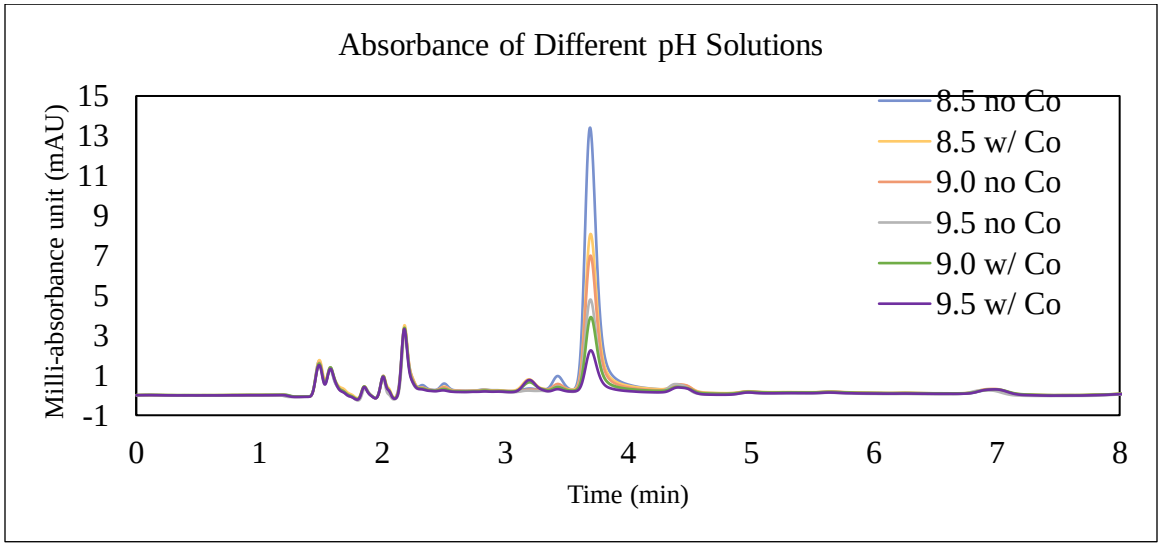

Figure 16. HPLC chromatograms of absorbance signals from solutions with different pH.

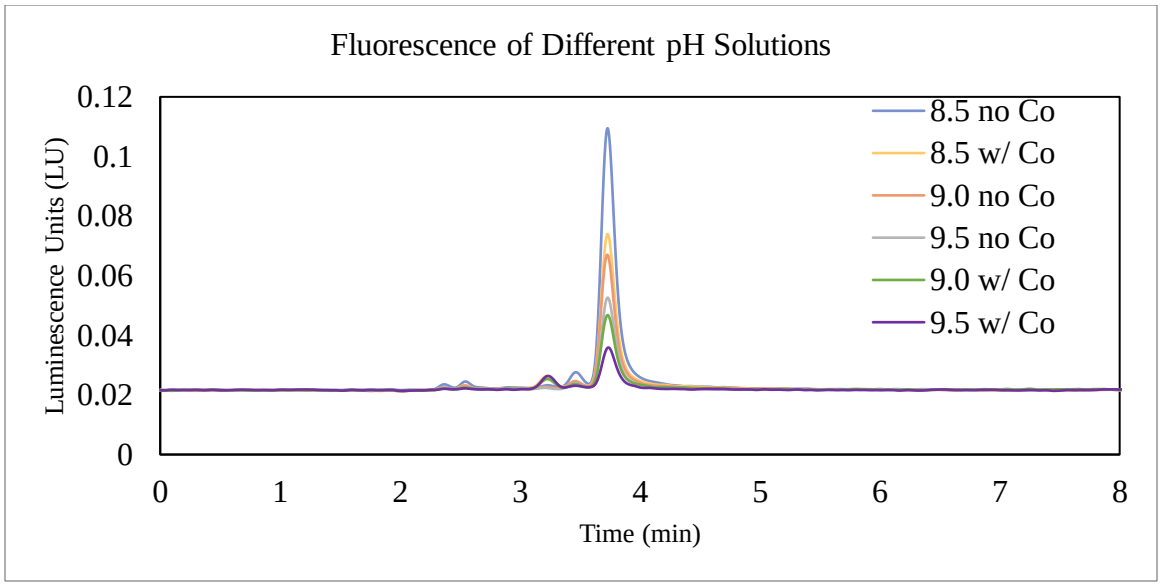

Figure 17. HPLC chromatograms of fluorescence signals from solutions with different pH.

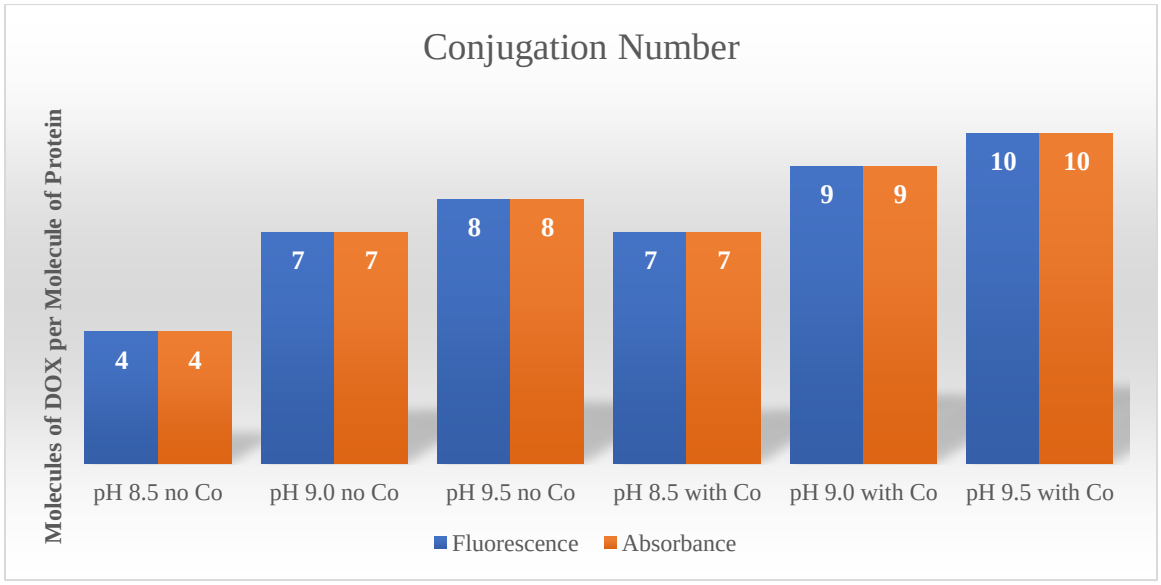

Figure 18. Conjugation number for change in pH.

The sample used to generate a calibration curve for this set of experiments was prepared with a sample of 200 µL of Dox HCl, 5 $\frac{mg}{mL}$, diluted with 2 mL of ultrapure

water. The pH was not adjusted in any way because in previous experiments it was found that the Dox did not freely diffuse into the bulk phase, but instead precipitated. The diffusion of Dox out of the cassette was evident by the color of the bulk phase (see Figure 19). The bulk phase and the sample inside the cassette had roughly the same color.

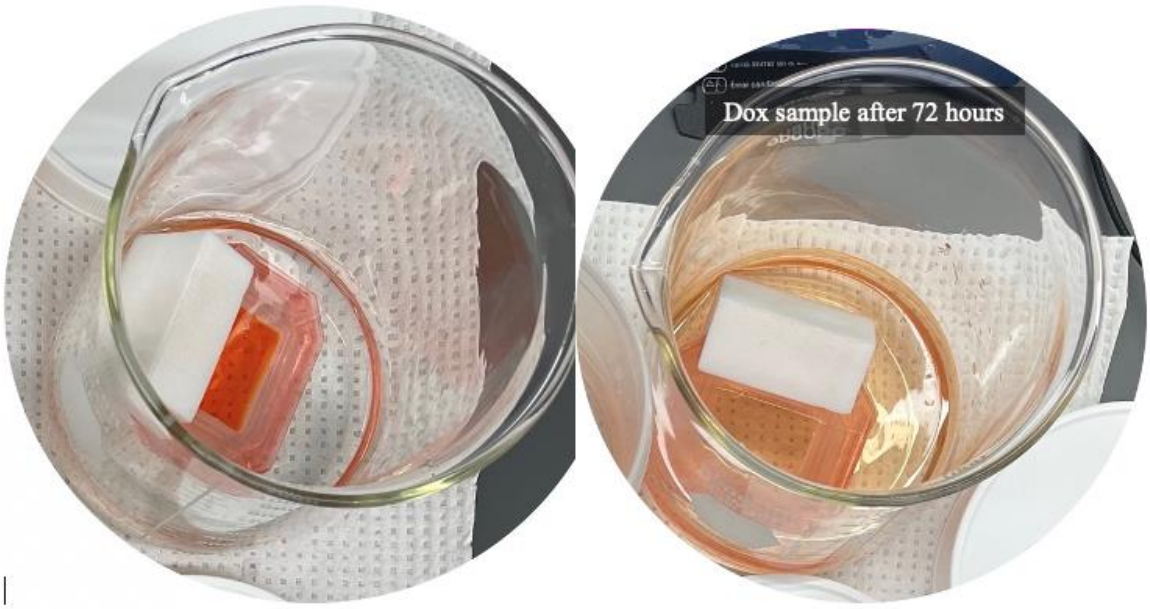

Figure 19. Dox-only samples. The left picture is the sample at the beginning of the experiment and the right picture is the sample after 72 hours.

The HPLC results from the bulk phase samples were in line with expectation (see Table 3). The area under the curve for the undiluted bulk phase for the Dox-only control was higher than the bulk phase from any of the conjugates. Figures 20–23 exhibit the result for the calibration curve performed for this experiment.

Table 3. HPLC Results from Different pH Samples

HPLC Results from Fluorescence Signals								
Sample	Dox added (mL)	Average Area	Concentration (μg/mL)	Dox Release in Bulk Phase (μg)	Total Dox in Cassette (μg)	Total Dox Retained in Cassette (μg)	% Retained	Molecules of DOX per Molecule of HSA
pH 8.5 no Co	0.2	0.71	3.38	683.0	1000	317.0	31.7	4
pH 9.0 no Co	0.2	0.38	1.91	384.9	1000	615.1	61.5	7
pH 9.5 no Co	0.2	0.26	1.39	280.5	1000	719.5	71.9	8
pH 8.5 with Co	0.2	0.43	2.14	432.6	1000	567.4	56.7	7
pH 9.0 with Co	0.2	0.21	1.17	235.8	1000	764.2	76.4	9
pH 9.5 with Co	0.2	0.12	0.75	152.4	1000	847.6	84.8	10
HPLC Results from Absorbance Signals								
Sample	Dox added (mL)	Average Area	Concentration (μg/mL)	Dox Release in Bulk Phase (μg)	Total Dox in Cassette (μg)	Total Dox Retained in Cassette (μg)	% Retained	Molecules of DOX per Molecule of HSA
pH 8.5 no Co	0.2	94.6	3.36	679.0	1000	321.03	32.1	4
pH 9.0 no Co	0.2	49.7	1.90	382.9	1000	617.15	61.7	7
pH 9.5 no Co	0.2	34.2	1.39	280.4	1000	719.59	72.0	8
pH 8.5 with Co	0.2	57.5	2.15	433.9	1000	566.15	56.6	7
pH 9.0 with Co	0.2	27.5	1.17	236.4	1000	763.56	76.4	9
pH 9.5 with Co	0.2	15.3	0.77	155.5	1000	844.46	84.4	10

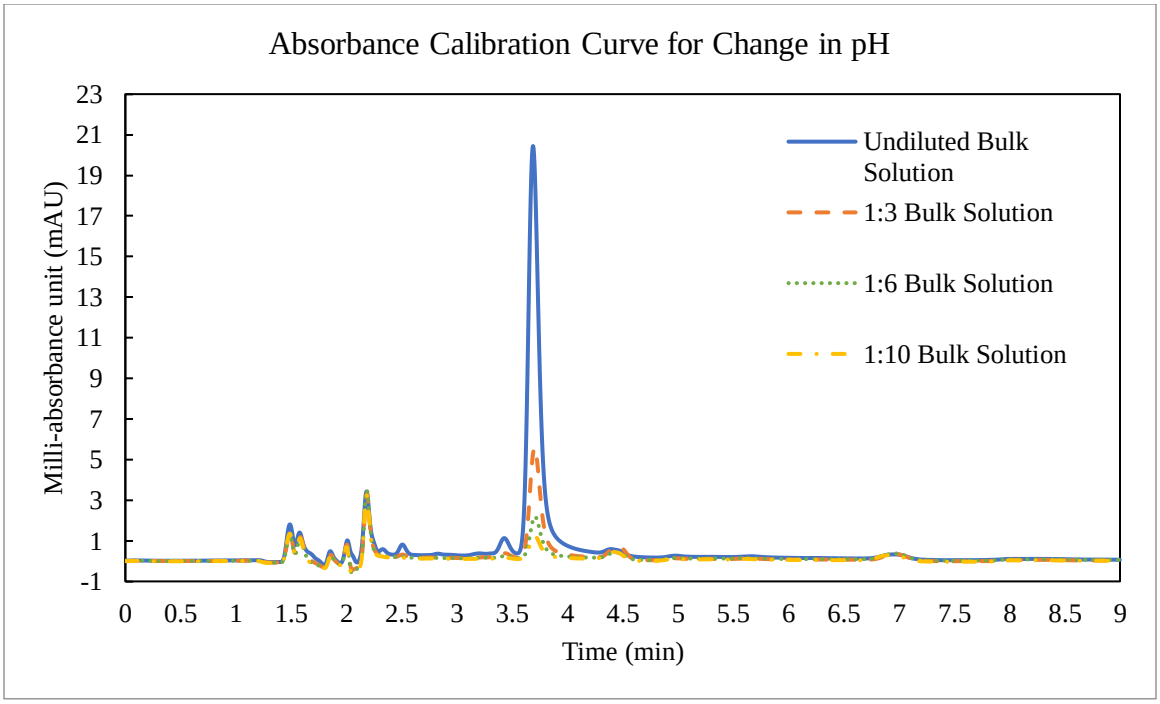

Figure 20. HPLC absorbance chromatograms for calibration curve of change in pH.

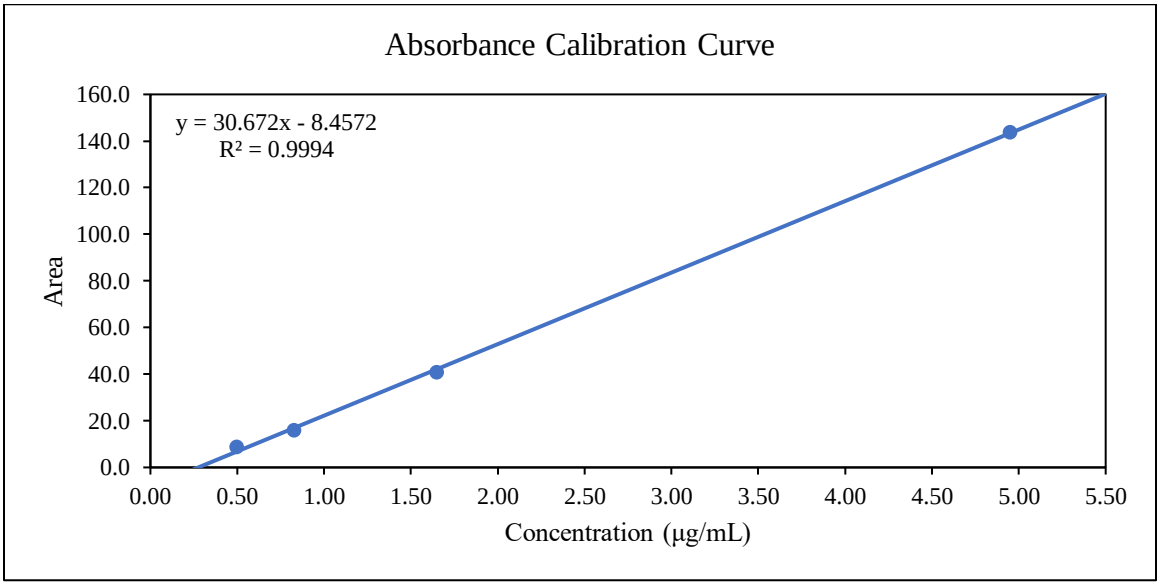

Figure 21. Absorbance calibration curve for change in pH.

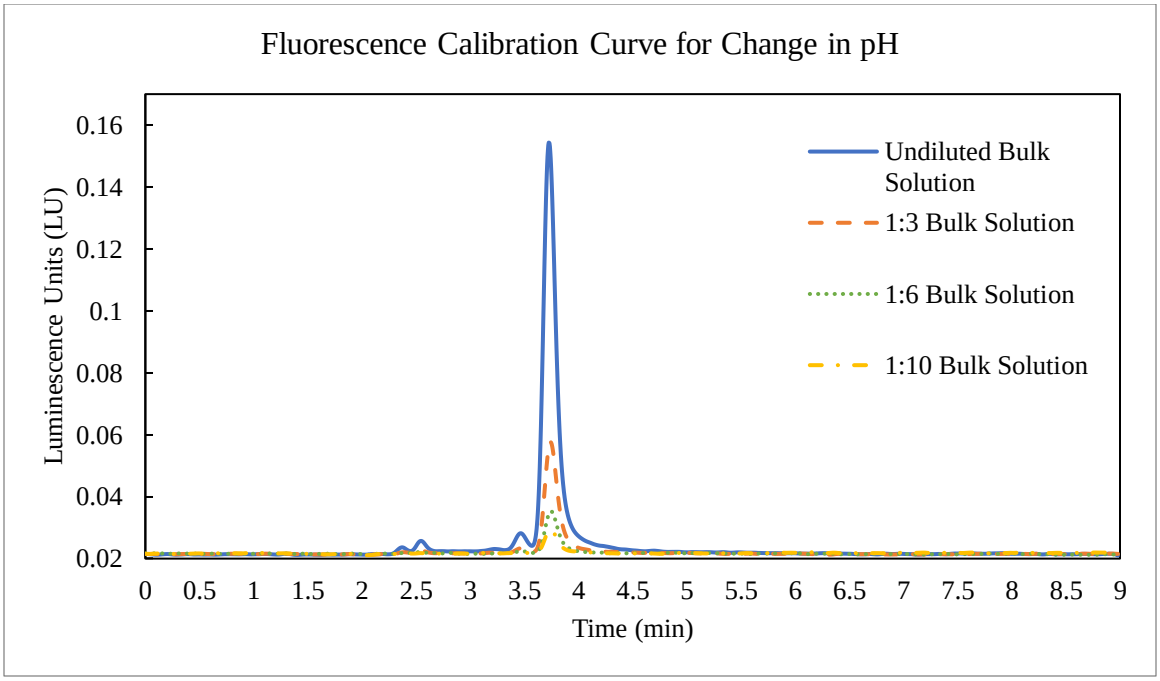

Figure 22. HPLC fluorescence detection chromatograms for calibration curve of change in pH.

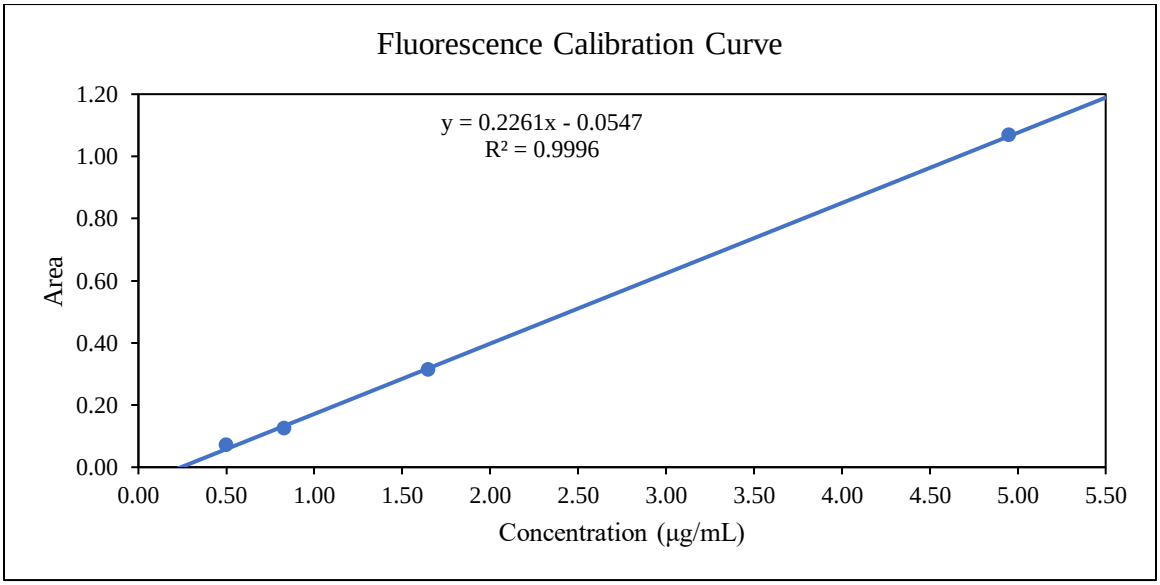

Figure 23. Fluorescence calibration curve for change in pH.

Change in Cobalt Concentration

The effects on the conjugation efficiency of the HSA-Dox conjugates were examined at varying cobalt concentrations. Cobalt served as the linker between HSA and Dox, so it was expected for the conjugation efficiency to increase at higher cobalt concentrations. The results did indicate an increase the number of Dox molecules/protein with the exception of the sample containing no cobalt, which was completely unexpected. The no cobalt control sample exhibited the highest retention of Dox (77.7%). There was an increase of 1 molecule of Dox/protein per 50% increase of cobalt concentration (see Table 4). The issue leading to the sample with no cobalt retaining the most Dox is discussed in the next chapter.

Table 4. HPLC Results from Change in Cobalt Concentration

HPLC Results from Fluorescence Signals								
Sample	Dox added (mL)	Average Area	Concentration (μg/mL)	Dox Release in Bulk Phase (μg)	Total Dox in Cassette (μg)	Total Dox Retained in Cassette (μg)	% Retained	Molecules of DOX per Molecule of HSA
0 μL Co	0.2	0.317	1.08	218.97	1000	781.03	78.1	9
26 μL Co	0.2	0.677	2.23	451.54	1000	548.46	54.8	6
52.5 μL Co	0.2	0.540	1.80	363.34	1000	636.66	63.7	7
78.5 μL Co	0.2	0.540	1.80	363.34	1000	636.66	63.7	7
105 μL Co	0.2	0.453	1.52	307.41	1000	692.59	69.3	8
HPLC Results from Absorbance Signals								
Sample	Dox added (mL)	Average Area	Concentration (μg/mL)	Dox Release in Bulk Phase (μg)	Total Dox in Cassette (μg)	Total Dox Retained in Cassette (μg)	% Retained	Molecules of DOX per Molecule of HSA
0 μL Co	0.2	43.53	1.10	223.20	1000	776.80	77.7	9
26 μL Co	0.2	91.30	2.29	463.94	1000	536.06	53.6	6
52.5 μL Co	0.2	72.70	1.83	370.26	1000	629.74	63.0	7
78.5 μL Co	0.2	71.63	1.80	364.93	1000	635.07	63.5	7
105 μL Co	0.2	61.20	1.54	312.38	1000	687.62	68.8	8

The absorbance chromatogram for the sample with 78.5 µL of Co added had an unusual peaks at around 1.8 minutes and 2.0 minutes (see Figure 24). These peaks were not present in the fluorescence chromatogram (see Figure 25). Some precipitate formed inside the cassettes. The precipitate was redispersed by agitating the solution, but it was observed to reform after the solution was left undisturbed. These precipitates were observed in the other experiments as well.

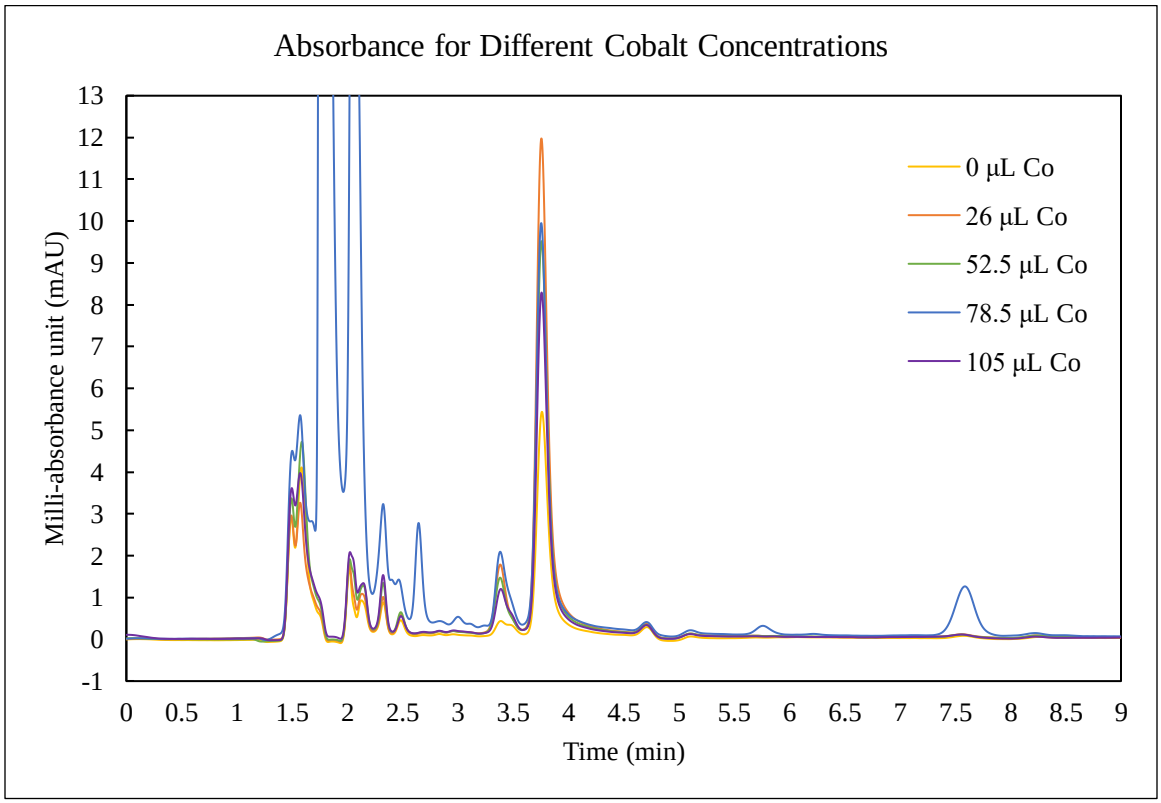

Figure 24. HPLC absorbance chromatograms from samples with different cobalt concentrations.

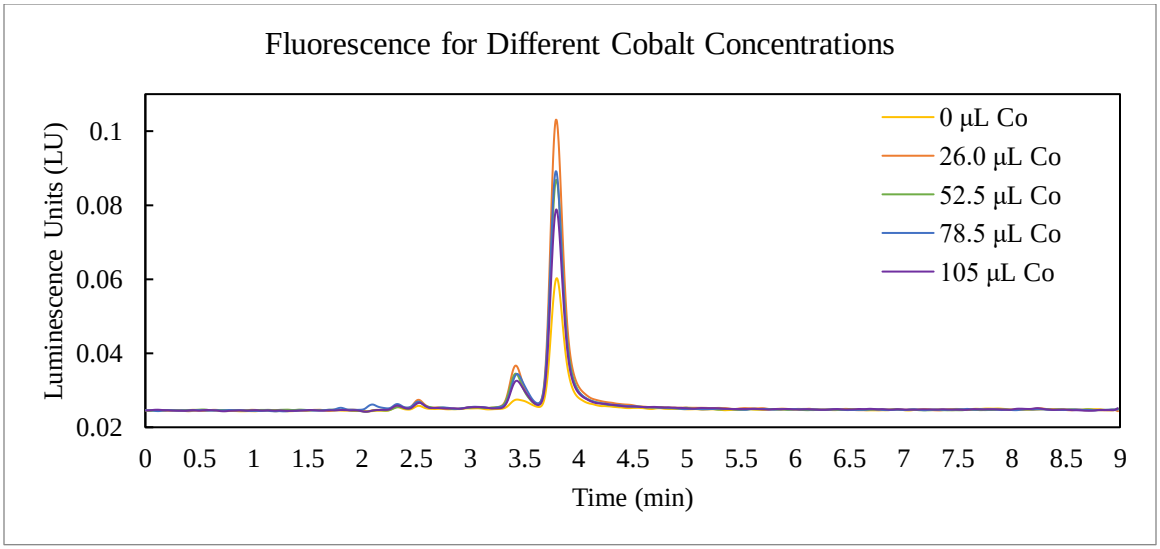

Figure 25. HPLC fluorescence detection chromatograms for samples with different cobalt concentrations.

The calibration curved was successfully generated for this experiment(see Table 5, Figures 26–28). Complete equilibrium between the sample inside the cassette and the bulk phase was noted by the uniformity in color, just like picture on the right in Figure 19.

Table 5. HPLC Result from Calibration Curve Samples for Change in Cobalt Concentration, Change in Dox Concentration, Synthesis of IgG, and Synthesis of Tf

Sample	Concentration (µg/mL)	Average Area from Absorbance Signals	Average Area from Fluorescence Signals
Undiluted Bulk	4.95	198.17	1.53
Bulk 1:3	1.65	64.33	0.47
Bulk 1:6	0.83	32.60	0.24
Bulk 1:10	0.5	19.70	0.14
Trendline Parameters			
Signals	Slope	Intercept	R^2
Absorbance	40.1288	-0.7629	0.99991
Fluorescence	0.3134	-0.0230	0.9995

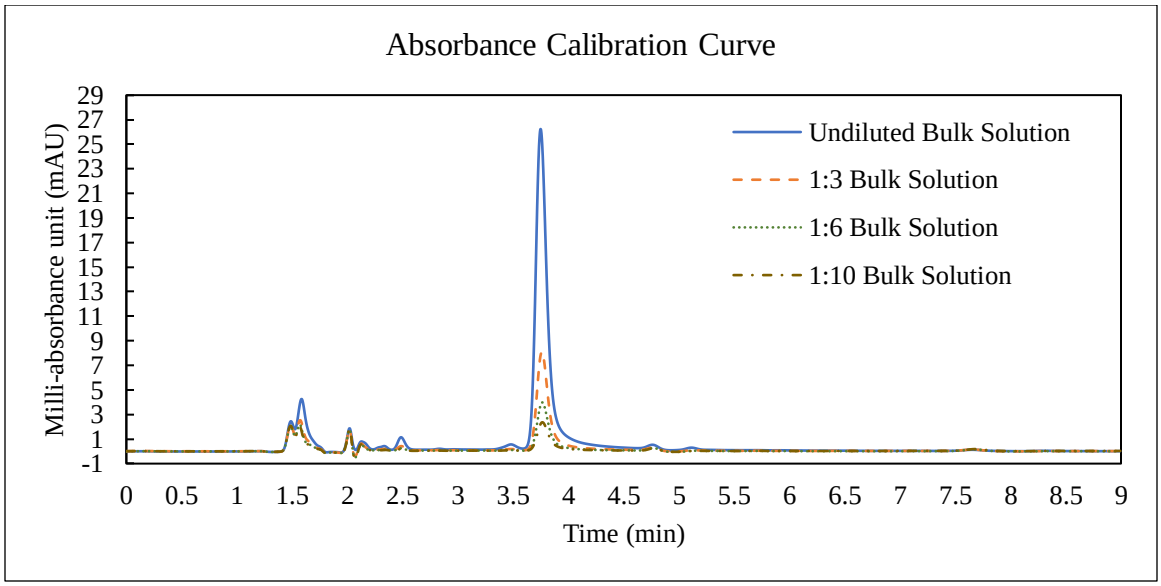

Figure 26. HPLC absorbance chromatograms of calibration curve for change in cobalt concentration, change in Dox concentration, synthesis of IgG, and synthesis of Tf.

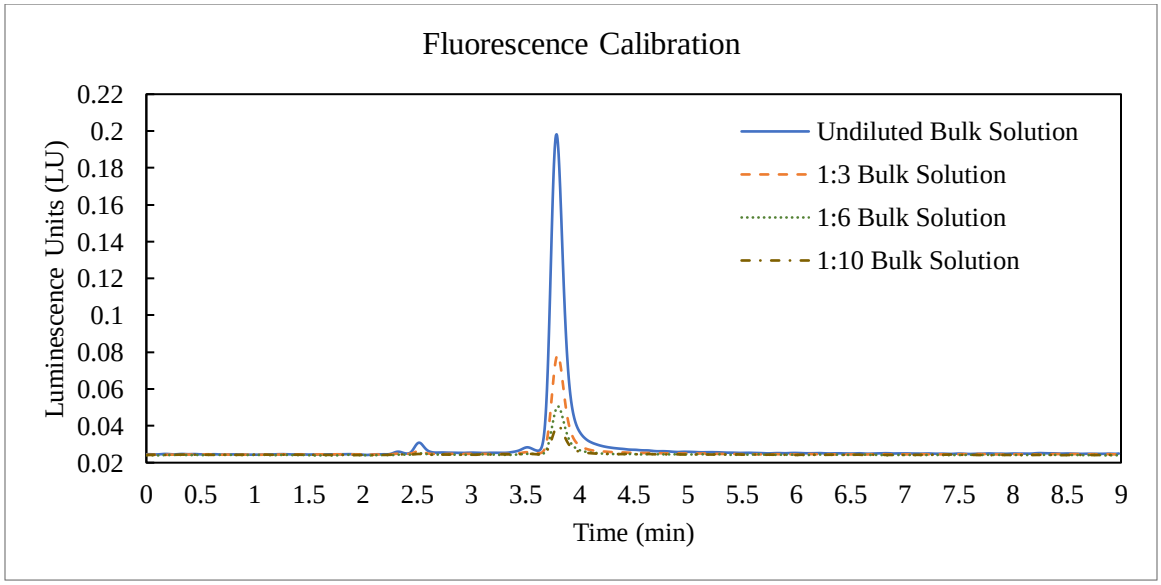

Figure 27. HPLC fluorescence detection chromatograms of calibration curve for change in cobalt concentration, change in Dox concentration, synthesis of IgG, and synthesis of Tf.

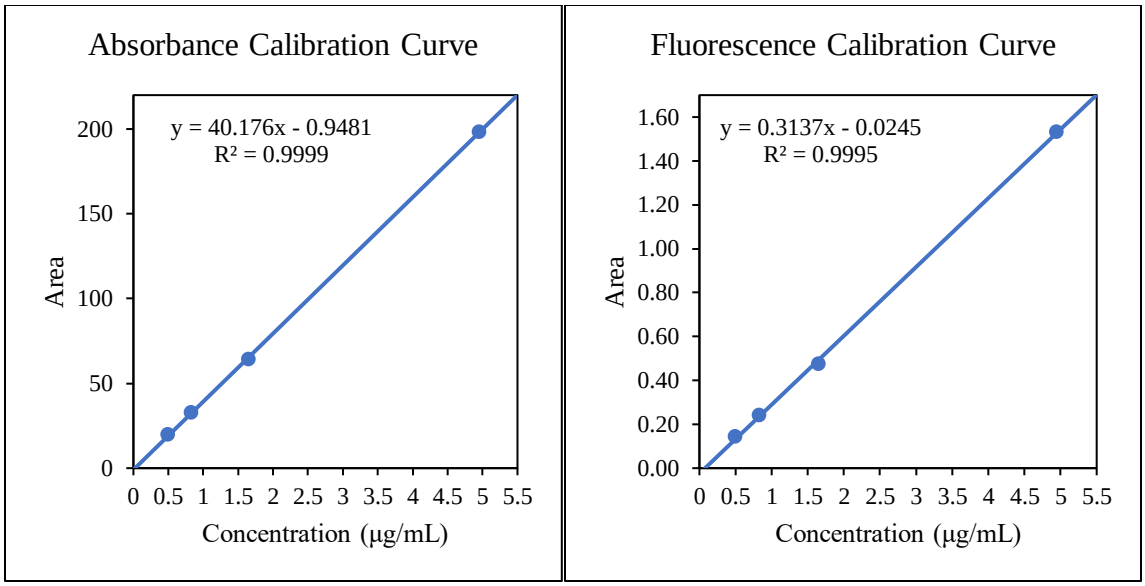

Figure 28. Absorbance (left) and fluorescence detection (right) calibration curves for change in cobalt concentration, change in Dox concentration, synthesis of IgG, and synthesis of Tf.

Change in Doxorubicin Concentration

Experiments were run at four different concentrations of Dox with the other parameters being held constant. It was expected that as the concentration of Dox increases the conjugation number increases because more molecules of Dox were available to react. The HPLC results (see Figures 29 and 30) were analyzed and they showed a proportional relationship between conjugation efficiency and the concentration of Dox, except for the first sample containing 50 µL of Dox (see Table 6). The conjugation number was doubled as the concentration was doubled. The calibration curve used for these experiments was the same as that used for the change in cobalt concentration experiment (the experiments were run concurrently).

Table 6. HPLC Results from Change in Dox Concentration

HPLC Results from Fluorescence Signals

Sample	Dox added (mL)	Average Area	Concentration (μg/mL)	Dox Release in Bulk Phase (μg)	Total Dox in Cassette (μg)	Total Dox Retained in Cassette (μg)	% Retained	Molecules of DOX per Molecule of HSA
50 μL Dox	0.05	0.025	0.15	30.76	250	219.24	87.7	3
100 μL Dox	0.1	0.290	1.00	201.93	500	298.07	59.6	3
200 μL Dox	0.2	0.680	2.24	453.75	1000	546.25	54.6	6
400 μL Dox	0.4	1.600	5.18	1048.57	2000	951.43	47.6	11

HPLC Results from Absorbance Signals

Sample	Dox added (mL)	Average Area	Concentration (μg/mL)	Dox Release in Bulk Phase (μg)	Total Dox in Cassette (μg)	Total Dox Retained in Cassette (μg)	% Retained	Molecules of DOX per Molecule of HSA
50 μL Dox	0.05	3.47	0.11	21.30	250	228.70	91.5	3
100 μL Dox	0.1	38.80	0.99	199.30	500	300.70	60.1	3
200 μL Dox	0.2	91.07	2.29	462.83	1000	537.17	53.7	6
400 μL Dox	0.4	207.77	5.20	1052.05	2000	947.95	47.4	11

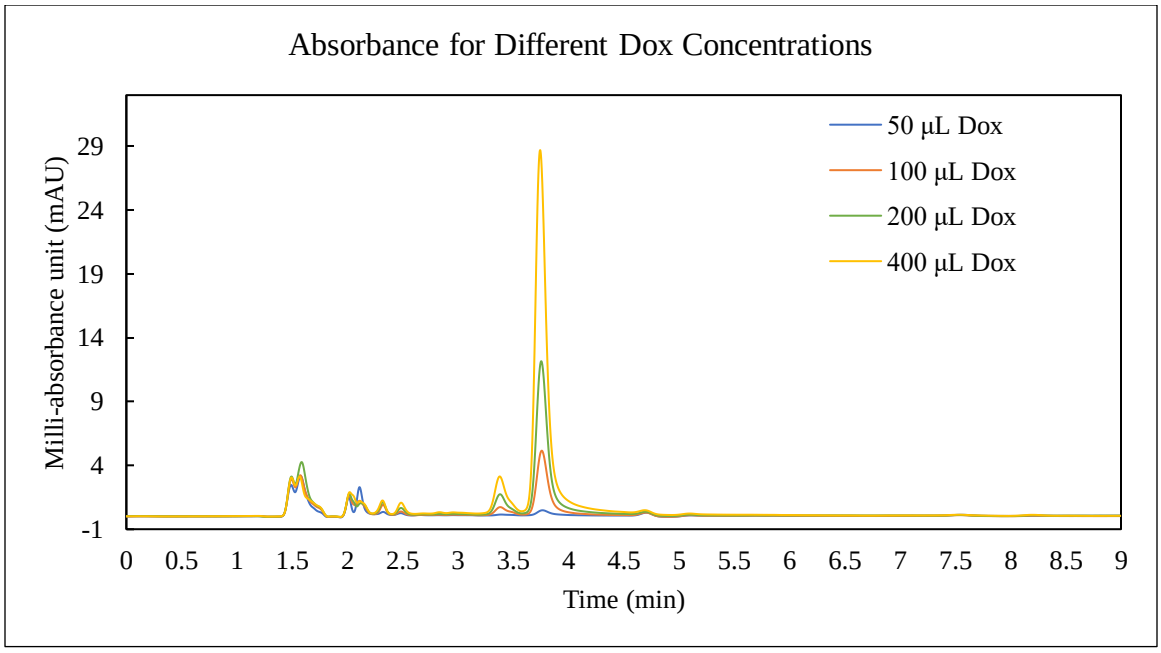

Figure 29. HPLC absorbance chromatograms from samples with different Dox concentrations.

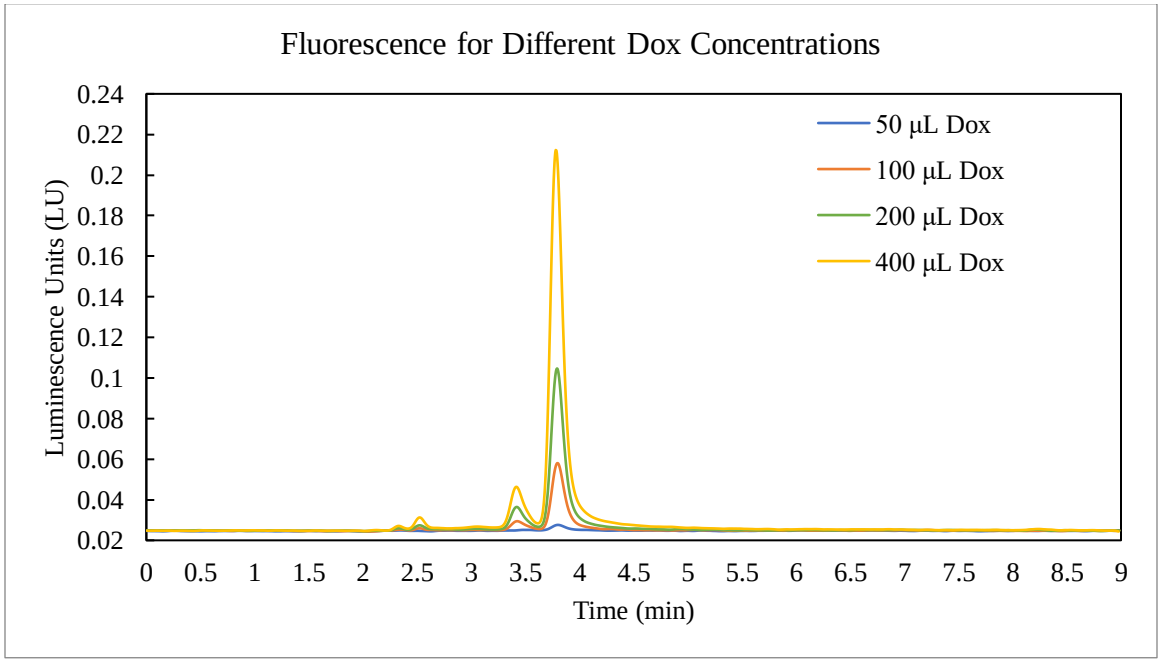

Figure 30. HPLC fluorescence detection chromatograms for samples with different Dox concentrations.

Tf-Dox Conjugate and IgG-Dox Conjugate

The Tf-Dox Conjugate and the IgG-Dox conjugate were successfully synthesized following the same preparation method as the HSA-Dox conjugate. The sample was then dialyzed for 72 hr followed by analysis via HPLC (see Figures 31 and 32, Table 7). Both newly synthesized conjugates had a slightly higher conjugation number (8 for Tf, and 11 for IgG) than the HSA-Dox (7). A tiny amount of red precipitate was also observed after 72 hours.

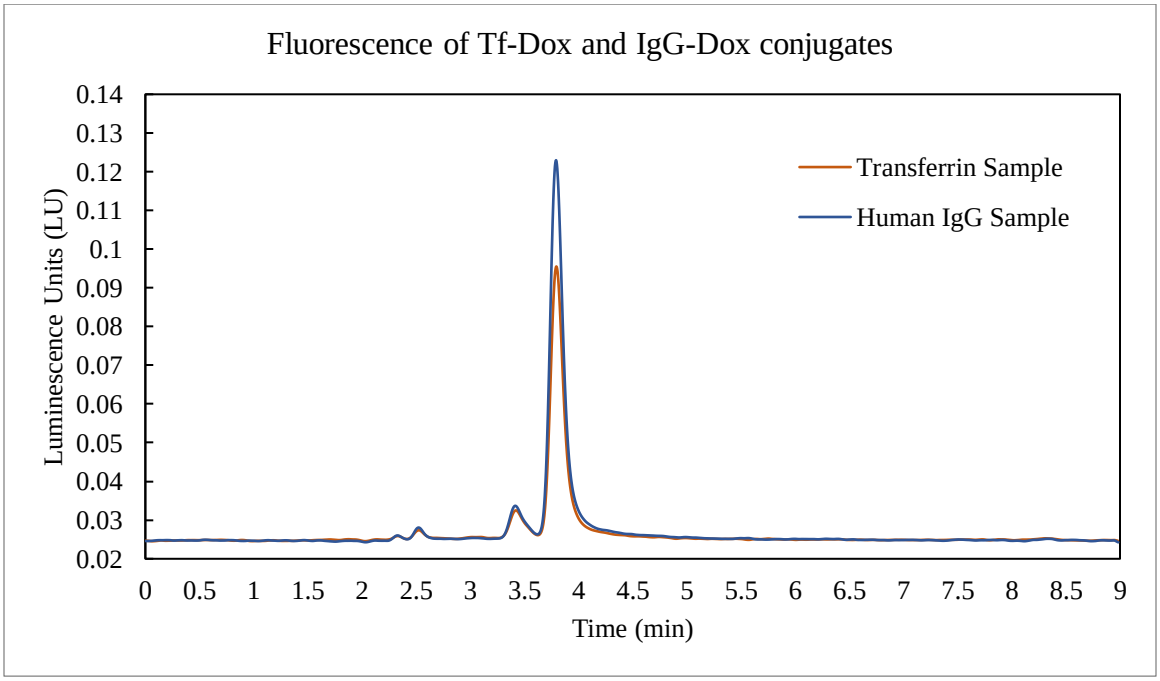

Figure 31. HPLC fluorescence detection chromatograms of bulk samples from IgG-Dox conjugate and Tf-Dox conjugate. The elution time of dox was at 3.8 min for both samples, but the dox peak of the IgG sample had a higher intensity.

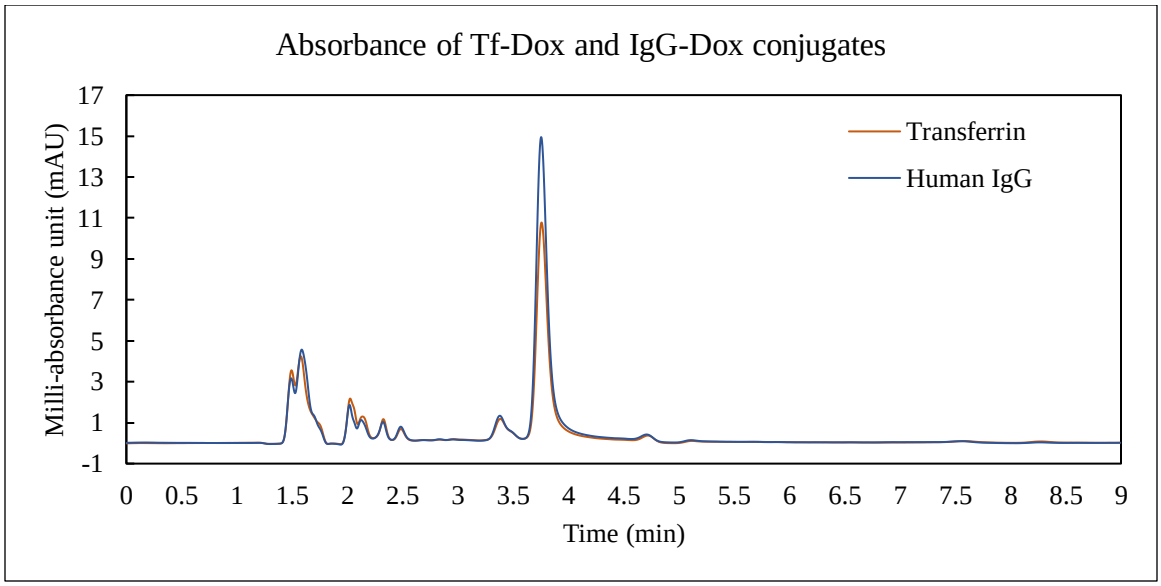

Figure 32. HPLC absorbance chromatograms of bulk samples from IgG-Dox conjugate and Tf-Dox conjugate. The elution time of dox was at 3.8 min for both samples, but the dox peak of the IgG sample had a higher intensity.

Table 7. HPLC Results from Synthesis of IgG-Dox Conjugate and Tf-Dox Conjugate

HPLC Results from Fluorescence Signals						
Sample	Dox added (mL)	Sample Average Area	Concentration (μg/mL)	Total Retained in Cassette (μg)	% Retained	Molecules of DOX per Molecule of Protein
IgG-Dox	0.2	0.87	2.85	424.34	42.4	11
Tf-Dox	0.2	0.61	2.01	594.09	59.4	8
HPLC Results from Absorbance Signals						
Sample	Dox added (mL)	Sample Average Area	Concentration (μg/mL)	Total Retained in Cassette (μg)	% Retained	Molecules of DOX per Molecule of Protein
IgG-Dox	0.2	116.83	2.93	408.04	40.8	11
Tf-Dox	0.2	81.47	2.05	586.07	58.6	8

Dynamic Light Scattering Studies

DLS studies were only performed for the samples at varying cobalt concentration (see Figures 33 and 34), varying Dox concentration samples, Tf-Dox conjugate, and IgG-Dox conjugate (see Figure 35). The HSA protein has a size of 6.4 nm × 5.5 nm × 5 nm.[29] The samples at varying cobalt concentration displayed similar sizes to the HSA protein. The samples at varying Dox concentrations also displayed similar sizes to the HSA protein (see Table 8). The consistency in the average particle size indicated the solutions consisted mostly of one size and shape of particle. The polydispersity index (PDI) is a measurement of the broadness of the size distribution. The ISO 22412:2017 states a PDI value of 0.07 or less means the sample is monodisperse, if the sample is composed of spherical particles. It is important to note the proteins used were not spherical. Values larger than 0.7 are common to polydisperse solutions.[30] Only two samples had PDI values above 0.7. This indicates the presence of aggregates in the solutions. All the solutions were observed to form a red precipitate after 72 hours. The precipitate in these solutions was probably the cause of the observed polydispersity in the samples and likely indicates protein aggregation.

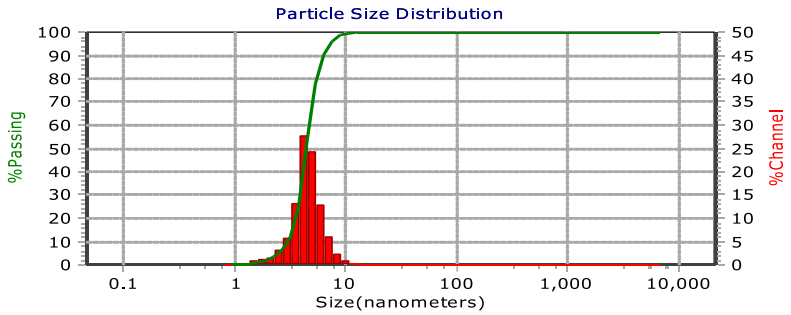

Figure 33. Particle size distribution of HSA-Dox conjugate with no cobalt.

Table 8. DLS Results[a]

Sample	MN (nm)	SD (nm)	PDI	Peaks Summary		
				Dia (nm)	Volume %	Width
Change in Co Concentration						
0 µL Co	4.65	1.18	0.553	4.43	100	2.37
26 µL Co	6.17	1.64	0.413	5.83	100	3.27
52.5 µL Co	5.47	1.66	0.2533	5.21	100	3.31
78.5 µL Co	5.74	1.34	0.1845	5.38	100	2.68
105 µL Co	4.23	1.34	0.1645	3.82	100	2.69
Change in Dox Concentration						
50 µL Dox	6.63	1.14	0.585	6.4	100	2.29
100 µL Dox	5.87	1.25	0.2475	5.49	100	2.51
200 µL Dox	4.67	1.2	0.808	4.43	100	2.4
400 µL Dox	6.47	1.84	0.867	5.99	100	3.68
IgG and Tf conjugates						
IgG-Dox	5.43	1.28	0.69	5.06	100	2.56
Tf-Dox	4.49	1.51	0.518	4.22	100	3.02

[a]MN is the mean number diameter, SD is the Standard Deviation, PDI is the polydispersity index, and Dia is the 50% point of each mode.

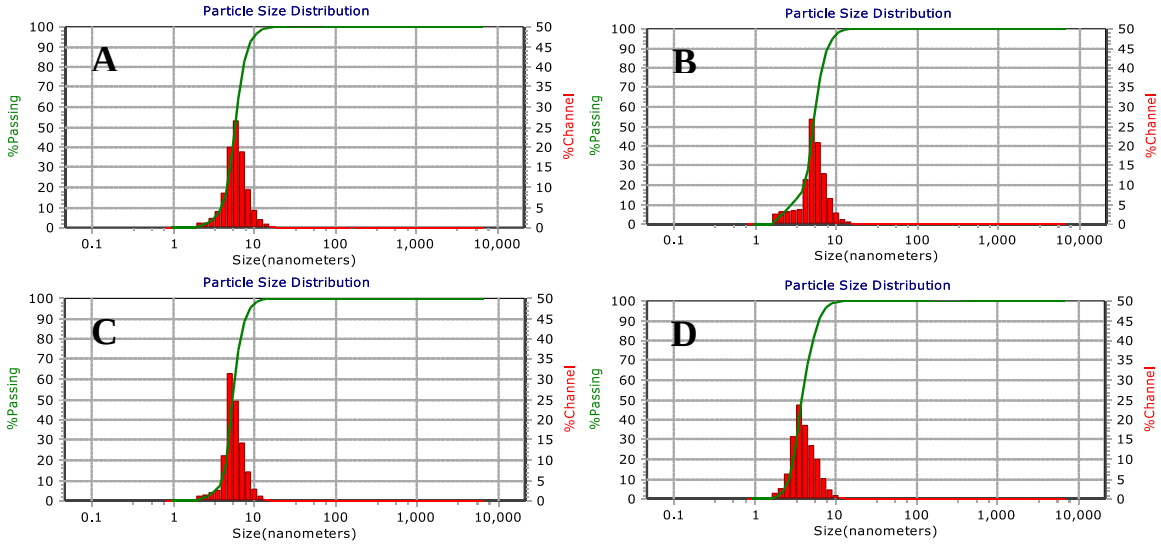

Figure 34. Particle size distribution of HSA-Dox conjugates with different amounts of cobalt, 26 µL Co (A), 52.5 µL Co (B), 78.5 µL Co (C), and 105 µL Co (D).

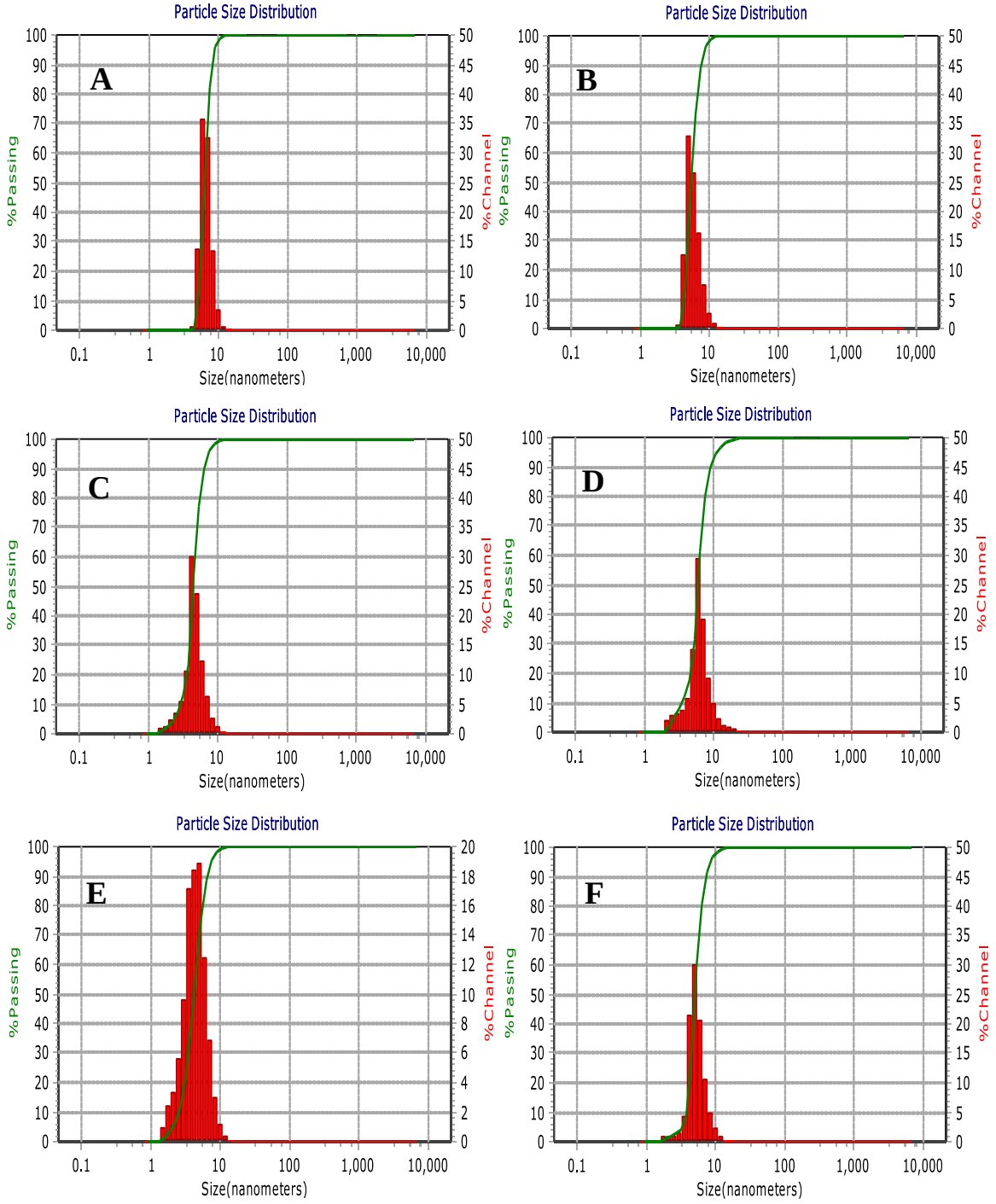

Figure 35. Particle size distribution of different concentration of Dox (A. 50 µL Dox, B. 100 µL Dox, C. 200 µL Dox, D. 400 µL Dox), Tf-Dox conjugate (E), and IgG-Dox conjugate(F).

Differential Scanning Calorimetry Study

The DSC study was performed to probe the stability of the newly synthesized conjugate. The study was only performed on the Tf-Dox conjugate. The increase in temperature causes the breakage of weak bonds, which results in the protein denaturing (unfolding) at a certain temperature known as the temperature of denaturation (T_m). The denaturation of the protein was observed as a single peak in the DSC thermogram (see Figures 36 and 37). The T_m of Tf protein only was found to be 84.80 ºC with an enthalpy of denaturation (ΔH) of 566.9 $\frac{KJ}{mol}$. The Tf-Dox conjugate was found to have a T_m of 84.83 ºC and a ΔH of 565.2 $\frac{KJ}{mol}$. The Tf-Dox conjugate had the same T_m and ΔH of the protein, which indicates the stability of the protein was likely retained throughout the experiment.

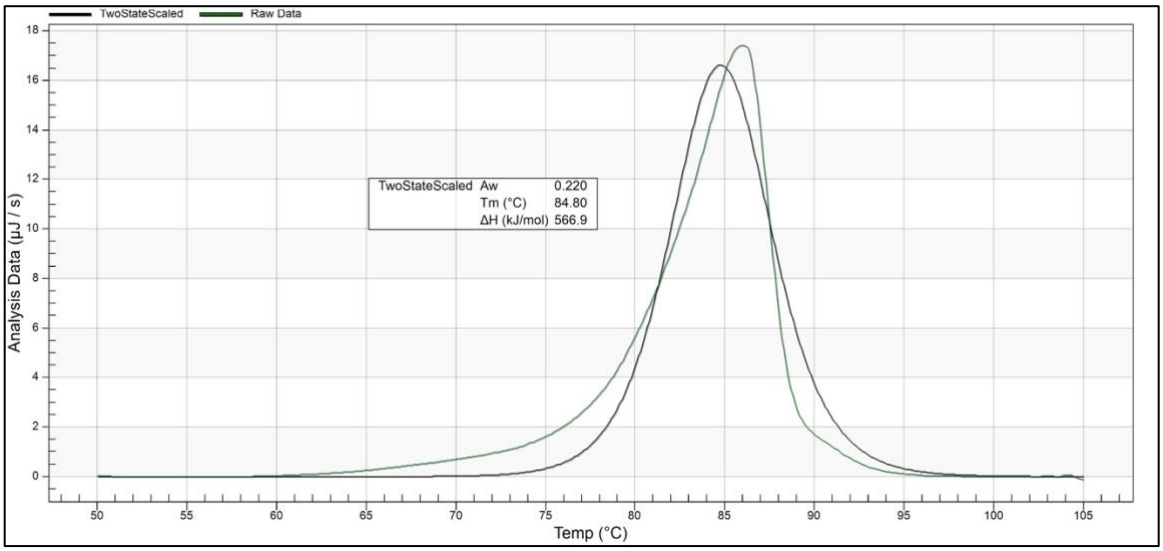

Figure 36. DSC thermogram of Tf protein. The green line is the raw data, and the black graph is the Two State Scaled model used to calculate the T_m (84.80 ºC) and ΔH (566.9 KJ/mol).

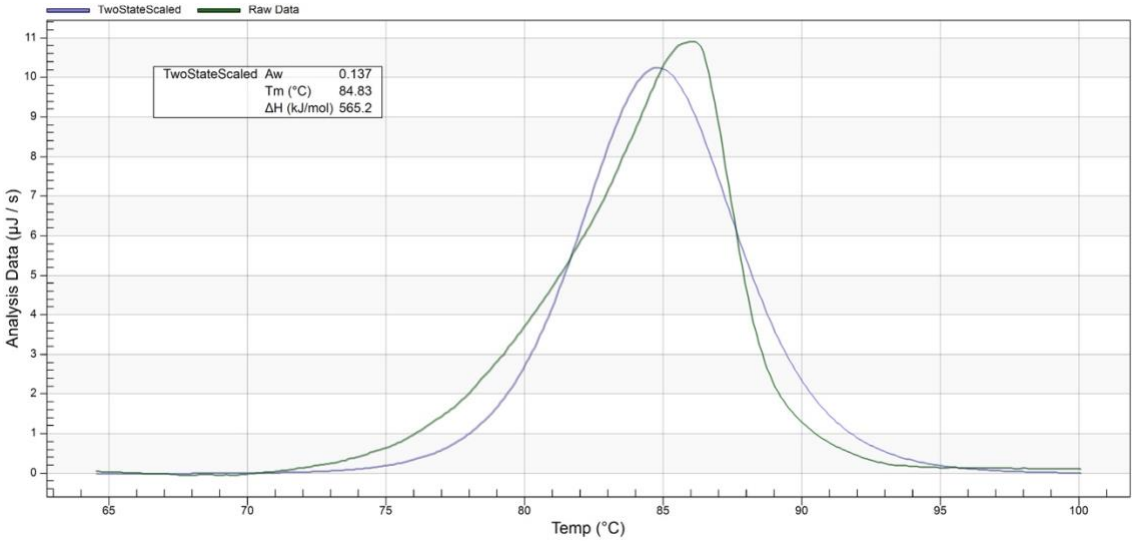

Figure 37. DSC thermogram of Tf-Dox conjugate. The green line is the raw data, and the black graph is the Two State Scaled model used to calculate the T_m (84.83 ºC) and ΔH (565.2 KJ/mol).

Cytotoxicity

The cell viability was tested in a human breast cancer cell line, MCF-7 cells, using an MTS mitochondrial function assay. Two samples of Dox were tested as a control. The concentration of Dox in the conjugate solutions was calculated based on the HPLC results (see Tables 4, 6, and 7). The initial conjugate solutions were diluted to a concentration of 35 µM Dox in solution, follow by a 10-fold dilution series. It was found the Tf-Dox conjugate and the HSA-Dox had a lower cytotoxity (IC_{50} = 168 µM) than the IgG-Dox conjugate (IC_{50} = 80 µM; see Figure 38). The results were promising, but more studies will need to be performed.

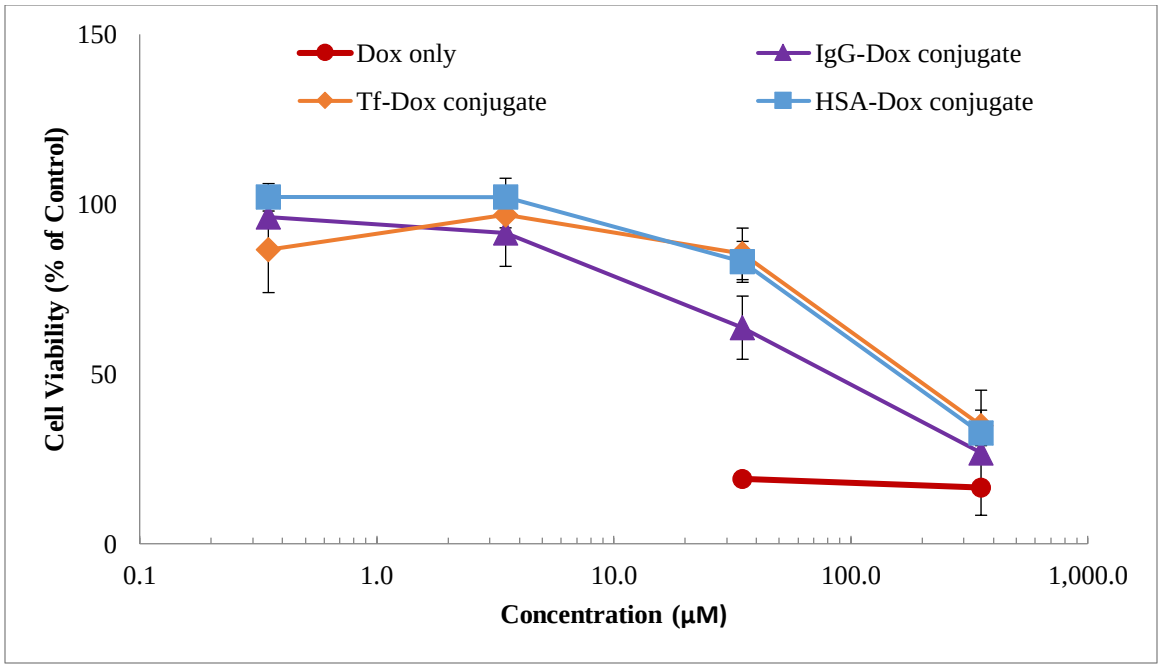

Figure 38. Cell viability studies of IgG-Dox conjugate, Tf-Dox conjugate, and HSA-Dox conjugate in MCF-7 cells with MTS assay.

CHAPTER IV

FINAL DISCOVERY

The expected trends were observed in virtually all the experiments conducted here; however, the red precipitate that continued to form in Dox-only controls or solution with no cobalt led to literature research pertaining to the stability of Dox in various solutions. This hypothesis was formed when the Dox calibration sample at adjusted pH would not diffuse out of the cassette. Whatever was happening in the case of the Dox-only sample could be occurring in all the conjugate samples. In one set of experiments where the pH of the Dox solution was increased first and left on the bench while adjusted the pH of the protein solution two layers in the Dox sample formed, a red precipitate and a clear red one. Another example was observed in Figure 15 when a red precipitated was observed inside the cassette after 10 days in PBS. A paper published in 2020 by Yuji Yamada[31] explains what was happening to Dox in these solutions. The red precipitate observed in these solutions was caused by the formation of a Dox dimer (see Figure 39). The Dox dimer forms in PBS it turns out, and is both temperature and pH dependent. The reaction occurs when the α-hydroxy ketone group of dox is deprotonated, this leads to the formation of an enediol which then undergoes keto-enol tautomerization to form an α-hydroxy aldehyde group. The α-hydroxy aldehyde group undergoes imine formation by the addition of the nitrogen group from another Dox molecule to form and α-hydroxy imine. Another tautomerization reaction takes place in the α-hydroxy imine to form an

enaminol which it goes oxidation to form the final product the α-iminoketone (the red precipitate).[31]

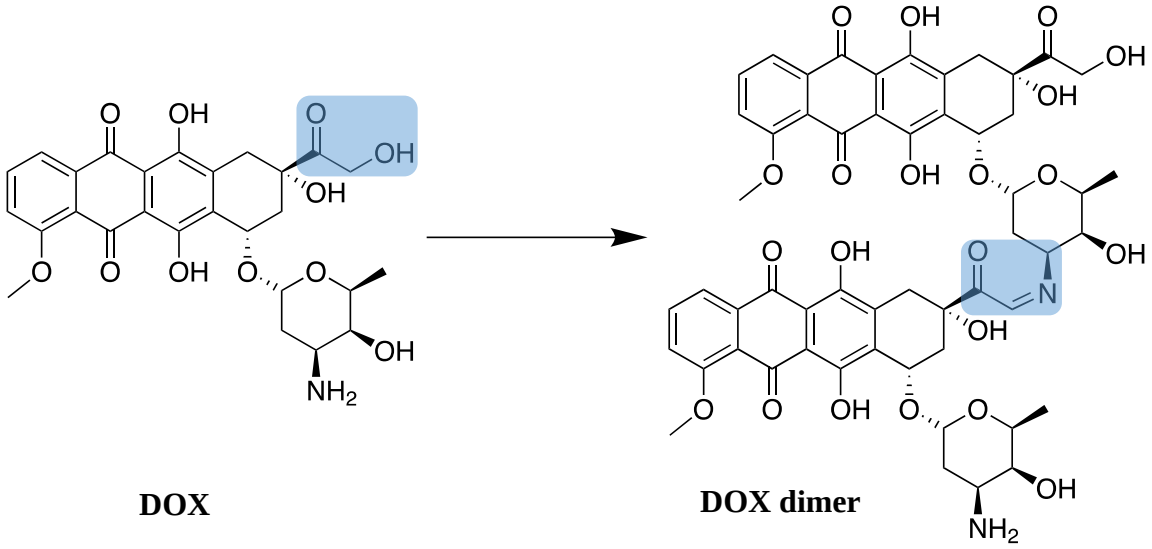

Figure 39. Dox and Dox dimer structures.

The samples used in this research had only a tiny amount of precipitate. This was confirmed by DLS as the median diameter of the conjugates matched the expected size. The polydispersity observed in the samples was caused by small amount of precipitate that formed. While the synthesis method described in this work, a new method needs to be developed to prevent the formation of Dox dimers. A solution to this could be changing the order of addition during formulation, which could diminish the formation of free amines in solution.

CHAPTER V

CLOSING STATEMENTS

An important lesson I learned throughout my research and my attendance at TWU was to think outside the box. This lesson has been helpful not only in my research, but also in personal aspects of life. Sometimes things could be easier than what we think if we look at them from a different perspective. The number of obstacles experienced throughout my research have been unbelievable, but at the end perseverance and motivation led the way. If I was able to do it, everyone should be able to do it too. You just have to believe in yourself. The support from faculty and the opportunities given to me, made my attendance at TWU a unique and unforgivable experience.

REFERENCES

1. Pass, H. A. Foreword. In *The Gale Encyclopedia of Cancer: A Guide to Cancer and Its Treatments*; Fust, K., Ed.; Gale: Farmington Hills, MI, 2015; Vol. 1, pp xi–xiii.

2. Siegel, R. L.; Miller, K. D.; Jemal, A. Cancer Statistics, 2020. *CA A Cancer J Clin.* **2020**, *70*, 7–30.

3. Ferlay, J.; Laversanne, M.; Ervik, M.; Lam, F.; Colombet, M.; Mery, L.; Piñeros, M.; Znaor, A.; Soerjomataram, I.; Bray, F. Global Cancer Observatory: Cancer Tomorrow. https://gco.iarc.fr/tomorrow (accessed Dec 1, 2020).

4. Carson-DeWitt, R.; Frey, R. J. Cancer. In *The Gale Encyclopedia of Medicine*; Longe, J. L., Ed.; Gale: Farmington Hills, MI, 2020; Vol. 2, pp 920–928.

5. Fruman, D. A.; O'Brien, S. Cancer: Targeted Treatment with Off-Target Risks. *Nature* **2017**, *542*, 424–425.

6. Haag, R.; Kratz, F. Polymer Therapeutics: Concepts and Applications. *Angewandte Chemie International Edition* **2006**, *45*, 1198–1215.

7. Petros, R. A.; DeSimone, J. M. Strategies in the Design of Nanoparticles for Therapeutic Applications. *Nature Reviews. Drug Discovery* **2010**, *9*, 615–627.

8. Desai, N. Challenges in Development of Nanoparticle-Based Therapeutics. *AAPS J.* **2012**, *14*, 282–295.

9. Pérez-Herrero, E.; Fernández-Medarde, A. Advanced Targeted Therapies in Cancer: Drug Nanocarriers, the Future of Chemotherapy. *Eur. J. Pharm. Biopharm.* **2015**, *93*, 52–79.

10. Bonadonna, G.; Monfardini, S.; de Lena, M.; Fossati-Bellani, F. Clinical Evaluation of Adriamycin, a New Antitumour Antibiotic. *Br. Med. J.* **1969**, *3*, 503–506.

11. National Center for Biotechnology Information. Doxorubicin Hydrochloride. https://pubchem.ncbi.nlm.nih.gov/compound/443939 (accessed Dec 01, 2020).

12. Carvalho, C.; Santos, R. X.; Cardoso, S.; Correia, S.; Oliveira, P. J.; Santos, M. S.; Moreira, P. I. Doxorubicin: The Good, the Bad and the Ugly Effect. *Curr. Med. Chem.* **2009**, *16*, 3267–3285.

13. Yang, F.; Teves, S. S.; Kemp, C. J.; Henikoff, S. Doxorubicin, DNA Torsion, and Chromatin Dynamics. *Biochimica et Biophysica Acta (BBA) - Reviews on Cancer* **2014**, *1845*, 84–89.

14. McGowan, J. V.; Chung, R.; Maulik, A.; Piotrowska, I.; Walker, J. M.; Yellon, D. M. Anthracycline Chemotherapy and Cardiotoxicity. *Cardiovascular Drugs and Therapy* **2017**, *31*, 63–75.

15. MacGillivray, R. T.; Mendez, E.; Sinha, S. K.; Sutton, M. R.; Lineback-Zins, J.; Brew, K. The Complete Amino Acid Sequence of Human Serum Transferrin. *Proc. Natl. Acad. Sci. U. S. A.* **1982**, *79*, 2504–2508.

16. Szwed, M.; Wrona, D.; Kania, K. D.; Koceva-Chyla, A.; Marczak, A. Doxorubicin–Transferrin Conjugate Triggers Pro-Oxidative Disorders in Solid Tumor Cells. *Toxicology in Vitro* **2016**, *31*, 60–71.

17. Wagner, E.; Cotten, M.; Mechtler, K.; Kirlappos, H.; Birnstiel, M. L. DNA-Binding Transferrin Conjugates as Functional Gene-Delivery Agents: Synthesis by Linkage

of Polylysine or Ethidium Homodimer to the Transferrin Carbohydrate Moiety. *Bioconjugate Chem.* **1991**, *2*, 226–231.

18. Sutar, Y. B.; Mali, J. K.; Telvekar, V. N.; Rajmani, R. S.; Singh, A. Transferrin Conjugates of Antitubercular Drug Isoniazid: Synthesis and In Vitro Efficacy. *Eur. J. Med. Chem.* **2019**, *183*, 111713.
19. Abdollahpour-Alitappeh, M.; Lotfinia, M.; Gharibi, T.; Mardaneh, J.; Farhadihosseinabadi, B.; Larki, P.; Faghfourian, B.; Sepehr, K. S.; Abbaszadeh-Goudarzi, K.; Abbaszadeh-Goudarzi, G.; et al. Antibody-Drug Conjugates (ADCs) for Cancer Therapy: Strategies, Challenges, and Successes. *J. Cell. Physiol.* **2019**, *234*, 5628–5642.
20. Chau, C. H.; Steeg, P. S.; Figg, W. D. Antibody–Drug Conjugates for Cancer. *Lancet* **2019**, *394*, 793–804.
21. Jain, N.; Smith, S. W.; Ghone, S.; Tomczuk, B. Current ADC Linker Chemistry. *Pharm. Res.* **2015**, *32*, 3526–3540.
22. Nguyen, D. T.; Cavazos, R. J.; Harris, A. N.; Petros, R. A. Werner Complexes Viewed Anew: Utilizing Cobalt Coordination Chemistry for 'Traceless' Stimuli-Responsive Bioconjugation Involving Therapeutic Nanoparticles, Protein PEGylation, and Drug-(Bio)polymer Conjugates. *Comments On Modern Chemistry. Part A, Comments on Inorganic Chemistry* **2014**, *34*, 59–77.
23. Munteanu, C. R.; Suntharalingam, K. Advances in Cobalt Complexes as Anticancer Agents. *Dalton Trans.* **2015**, *44*, 13796–13808.

24. Graf, N.; Lippard, S. J. Redox Activation of Metal-Based Prodrugs as a Strategy for Drug Delivery. *Adv. Drug Deliv. Rev.* **2012**, *64*, 993–1004.

25. Motlagh, N. S. H.; Parvin, P.; Ghasemi, F.; Atyabi, F. Fluorescence Properties of Several Chemotherapy Drugs: Doxorubicin, Paclitaxel and Bleomycin. *Biomedical Optics Express* **2016**, *7*, 2400–2406.

26. Basu, D.; Mazumder, S.; Niklas, J.; Baydoun, H.; Wanniarachchi, D.; Shi, X.; Staples, R. J.; Poluektov, O.; Schlegel, H. B.; Verani, C. N. Evaluation of the Coordination Preferences and Catalytic Pathways of Heteroaxial Cobalt Oximes Towards Hydrogen Generation. *Chem. Sci.* **2016**, *7*, 3264–3278.

27. Lorber, B.; Fischer, F.; Bailly, M.; Roy, H.; Kern, D. Protein Analysis by Dynamic Light Scattering: Methods and Techniques for Students. *Biochem. Mol. Biol. Educ.* **2012**, *40*, 372–382.

28. Gill, P.; Moghadam, T. T.; Ranjbar, B. Differential Scanning Calorimetry Techniques: Applications in Biology and Nanoscience. *Journal of Biomolecular Techniques: JBT* **2010**, *21*, 167–193.

29. Wiwanitkit, V. Glomerular Pore Size Corresponding to Albumin Molecular Size, An Explanation for Underlying Structural Pathology Leading to Albuminuria at Nanolevel. *Ren. Fail.* **2006**, *28*, 101.

30. Mudalige, T.; Qu, H.; Van Haute, D.; Ansar, S. M.; Paredes, A.; Ingle, T. Characterization of Nanomaterials: Tools and Challenges. In *Nanomaterials for*

Food Applications; López Rubio, A., Fabra Rovira, M. J., martínez Sanz, M. and Gómez-Mascaraque, L. G., Eds.; Elsevier: 2019; pp 313–353.

31. Yamada, Y. Dimerization of Doxorubicin Causes Its Precipitation. *ACS Omega.* **2020**, *5*, 33235–33241.